SCINTILLATION SPECTROMETER STUDIES OF THE GAMMA-RADIATION FROM CARBON PLUS PROTON REACTIONS

Thesis by

H. Hugh Woodbury

In Partial Fulfillment of the Requirements

For the Degree of

Doctor of Philosophy

California Institute of Technology

Pasadena, California

1953

ACKNOWLEDGMENTS

I am happy to acknowledge the cooperation and much appreciated help of my many associates. Especially am I indebted to those who took the time to explain and interpret theoretical ideas and formulae. In this respect, I would like particularly to acknowledge Dr. R. G. Thomas for his assistance in the calculation of coulomb penetration factors and Alfred A. Kraus, Jr., for the use of his tables of Clebsch-Gordan coefficients and his patience in teaching me to use them.

I am indebted to Dr. Robert B. Day for instructing me in the use of the 3 Mev Electrostatic Generator, and for the privilege of being able to collaborate with him on much of the work reported in this thesis. Also, I wish to thank Dr. J. Thirion who assisted me in taking data and who performed some coincidence experiments for me.

It is a pleasure to acknowledge Professors C. C. Lauritsen, W. A. Fowler, R. F. Cristy, and T. Lauritsen for their willingness to listen to the troubles that one always encounters in such work as described in this thesis, and for their many suggestions on experiments and techniques.

Last of all, I wish to express my appreciation to Dr. A. V. Tollestrup who was instrumental in bringing about the research program which I followed. He not only suggested the original problem, but took the time to assist me in setting up the first equipment that was used. At all times he was willing to discuss problems, and was always actively interested in the work.

ABSTRACT

An efficient NaI(Tl) scintillation gamma-ray spectrometer is described, and its theoretical and experimental characteristics are given for gamma-ray energies from 0.5 Mev to 10 Mev. This spectrometer was used to measure the gamma-radiation from two proton-induced reactions. Presentation of the analysis of the data obtained at seven resonances of the first reaction, $C^{13}(p,\gamma)N^{14}$, is followed by a discussion on the energy levels in N^{14}. The results obtained for the second reaction, $C^{12}(p,\gamma p')C^{12}$, are likewise given, and are followed by a brief descriptive theory of the reaction.

TABLE OF CONTENTS

PART I

INTRODUCTION

Because of its relatively high efficiency, the scintillation counter has received considerable attention in the past few years as a device to measure high energy x-rays and nuclear decay products. One such counter introduced by Hofstadter and McIntyre[1], using a thallium-activated sodium iodide crystal (designated NaI(Tl)) and an end cathode photo-multiplier tube (RCA type 5819), has provided a means of doing gamma-ray spectroscopy on reactions an order of magnitude weaker than heretofore possible.

This thesis is concerned with the problem of using such a spectrometer to measure weak proton capture radiation, and of some results obtained from the capture of protons by carbon. In Part II, the basic principles underlying the NaI(Tl) scintillation spectrometer will be presented so as to provide an understanding of and an interpretation for the experimental results presented in Parts III and IV. Also in Part II, the pertinent experimental details will be presented on those items that were developed in the course of the work, and the general electronic problems and conditions associated with the spectrometer will be mentioned. In general, the discussion will be restricted to a phenomenological description of only the NaI(Tl) scintillation spectrometer. Thus the NaI(Tl) crystal will be referred to as, the crystal, and NaI(Tl) scintillation counter or spectrometer will be shortened to, counter.

PART II

THE NaI(Tl) SCINTILLATION SPECTROMETER

A. Basic Principles in the Operation of the NaI(Tl) Scintillation Spectrometer

The following processes or events are sufficient to explain the observed pulse-height spectrum from the counter for gamma-rays up to 10 Mev in energy.

Primary interactions

1. Photo-electric process
2. Compton interaction
3. Pair production

Secondary processes

1. Interaction with the crystal of the scattered photon from a primary Compton event.
2. Interaction of one or both of the annihilation quanta from the decay of a pair-produced positron.
3. Bremsstrahlung
4. Escape of fast electrons from the crystal (edge effect).

Although possibly causing some confusion, the term secondary electrons will be used in the usual sense to denote the energetic electrons produced directly by a primary event.

In brief, the principle of the counter is as follows. The primary interactions produce secondary electrons which

excite the crystal lattice causing light to be emitted. This light is then quantitatively measured with a photo-multiplier tube. It has been found experimentally that this light is proportional to the energy lost in the crystal. Since the photo-multiplier tubes can be operated so that their output is proportional to the light input, the final signal from the photo-multiplier, an electrical pulse, is proportional in size to the energy lost in the crystal. Thus if the secondary electrons are completely stopped in the crystal, the output will be related "proportionally" to the initial gamma-ray energy. While this proportionality is not necessary for the use of the counter, it is, nevertheless, a very desirable feature. In the discussion that follows, this proportionality will be implicitly assumed, that is, the size of the pulse out of the photo-multiplier tube will often be used interchangeably with energy-loss in the crystal.

The cross-sections for the primary processes are given in Figure 1, from which it is seen that the photo-electric and Compton effects are the important primary events for gamma-rays with energy less than 1.5 Mev. These curves are based on calculations made by Mr. A. Thiele, and have been checked against the work of Davisson and Evans[2]. In the photo-electric process (or in brief, the photo process), the total energy of a gamma-ray is transmitted to an electron which will produce an output signal proportional to the

gamma-ray energy. It is to be noted that the binding energy of the electrons is not important in so far as the proportionality of the device is concerned since the x-rays emitted when the "holes" are filled, are promptly absorbed by the crystal. Thus, when monoenergetic gamma-rays are being observed, a peak will occur in the differential pulse-height distribution corresponding to this photo interaction and hence to the full energy of the gamma-rays.

The Compton interaction produces electrons with energies ranging from zero to a maximum given by

$$E_e(\max) = E\ (1 + m_o c^2/2E)^{-1}$$

where $m_o c^2$ is the rest-energy of the electron (0.511 Mev). At low gamma-ray energies (less than 1 Mev), the energy distribution of the secondary Compton electrons rises at zero electron energy. At higher gamma-ray energies it is quite flat at low electron energies. At all gamma-ray energies, the distribution of the secondaries rises at high electron energies until the maximum energy is reached whence it breaks sharply. This rise and sharp break (the Compton peak) is not very pronounced in the counter because of the finite resolution which spreads out the sharp break and because of the capture of the scattered photon by the crystal. The probability for capture happening, is fairly high in this case because the scattered photons corresponding to the theoretical peak have an energy of 255 Kev (extreme relativistic case) or less. When this occurs so that the

full energy of the scattered photon is caught by the crystal (which again is very probable because of the low energies involved), the full energy of the gamma-ray is transmitted to the crystal. The output pulse corresponds in size to the photo-peak and cannot be differentiated from it.

For gamma-rays of energy higher than 1.5 Mev, pair production becomes important and it predominates above 7 Mev. The primary event in pair production is the creation of a positron and an electron, the sum of whose kinetic energies is $2m_0c^2$ less than the incident gamma-ray energy. If this were the only event, there would result a single peak (the pair peak) in the differential pulse-height spectrum corresponding to an energy of $2m_0c^2$ less than the full energy of the incident gamma-ray. However, when the positron decays into two 0.511 Mev quanta, there is a good chance that one of the annihilation quanta is captured and a smaller probability that both will be captured. The first possibility would give rise to a peak corresponding to an energy m_0c^2 less than the full energy (pair-plus-one peak). The second would give a peak corresponding to the full energy (pair-plus-two peak) which, again, cannot be differentiated from the photo-peak.

At high energies (10 Mev and above) the production of bremsstrahlung by the secondary electrons becomes important. The escape from the crystal of some of this bremsstrahlung, results in making the pair-peak asymmetrical in the 10 Mev

region, and completely smearing any structure for gamma-rays around 20 Mev(3).

If a secondary electron is formed within the electron's range of the edge of the crystal, there is a chance that it will escape without giving all its energy to the crystal. Over distances corresponding to the electron range for the energies considered here, the probability of a primary event is the same. Thus, assuming the range of an electron to be linearly dependent on its energy, equal numbers of electrons per unit energy will escape with energies from zero to the maximum energy. Hence, for monoenergetic radiation, this edge-effect gives rise in the output of a constant pulse-height distribution from zero to a maximum corresponding to the full energy of the radiation. For energies above 3 Mev, the range of the secondary electrons in NaI is approximately given by

$$R = 1.5\ E$$

where R is the range in millimeters and E is the energy of the electrons in Mev. This edge-effect can be roughly estimated for a given energy by comparing the range with the linear dimensions of the crystal used. Although the range of the secondaries is not exactly linear with energy, the prediction of the flat distribution based on this assumption appears to be correct for energies where the effect is important (see below).

The effects of these various processes, are shown in

Figures 2, 3, and 4 for a crystal 1.5 inches long by 1.5 inches in diameter. This size was the largest and most frequently used in these investigations. All of these figures have been normalized to the same area, with 10 on the abscissa corresponding to the full energy of the gamma-ray. In Figure 2, the Compton tail for the two cases shown (Cs^{137} and Na^{22} which gave 0.661 Mev and 1.277 Mev radiation respectively), has been calculated from the Klein-Nishina formula. For the higher energy cases shown in Figures 3 and 4, the tails have been idealized by continuing them constant back to the ordinate. Calculations using the Klein-Nishina formula and the above discussion on the edge-effect, indicate that this idealized constant tail for gamma-rays with energies above 1.5 Mev is a fairly accurate representation of the actual situation. This flat tail has been verified experimentally as far as it has been possible to do so (down to approximately 2 Mev for the 6 and 9 Mev radiation). It is impossible to measure the tail all the way to zero pulse-height because of background, other lower energy gamma-rays that may be present, annihilation radiation from pairs produced in the material around the crystal, or Compton photons scattered from such material. This latter effect is shown dotted in Figure 2, for Cs^{137}. As can be seen, it could be mistaken for a low energy gamma-ray. It is also seen in Figure 2 that the Compton peak for Cs^{137}, is completely removed by the secondary

process of the capture of the scattered photon as described above. This process considerably enhances the photo or full energy peak for large and moderately large crystals. Indeed, the photo-peak shown in Figure 3 for ThC" (2.615 Mev), is due in large part to this effect.

From Figure 3, the pair and pair-plus-one peaks can be seen to be just measurable at 1.65 Mev while at 2.615 Mev the pair-peak is nearly as large as the photo-peak, and is as useful for energy measurements.

Figure 4 shows the pair-process predominating for 6.13 Mev radiation with the resolution just sufficient to separate the pair and pair-plus-one peaks. For 9.17 Mev radiation (also Figure 4), the pair and pair-plus-one peaks cannot be resolved. Experimentally, however, it is found that for crystals up to the maximum size used in this work, the pair-peak energy is properly given by the maximum of this asymmetric peak. It is also seen here that the tail has appreciably increased at 9.17 Mev whereas the Compton cross-section continually drops with energy. This is due to the edge-effect which becomes important at these energies for this size crystal. Finally, the asymmetry on the back side of the pair-peak for the 9.17 Mev curve, is to be noted. This is due to the escape of some low energy bremsstrahlung as explained above.

For energies above 2 Mev, it is sometimes advantageous to use a smaller crystal to reduce the secondary processes.

For example, a smaller crystal (1/2-inch cube) for 6.13 Mev radiation would show very little structure of a pair-plus-one peak. It would, in fact, give a spectrum much like the 9.17 Mev spectrum shown in Figure 4. Using a smaller crystal, of course, reduces the overall efficiency of the counter. Also, the edge-effect is proportionally increased which effect limits the minimum size of the crystal.

It should be noted that whether a pulse is produced, is determined by whether a primary interaction has occurred. The particular interaction and the secondary effects, determine only the size of the pulse. Thus, the total number of pulses is proportional only to the total cross-section for the primary events. This fact is important when making absolute yield measurements where the efficiency of the counter as a function of energy must be either measured or calculated. A calculation of the efficiency for the particular geometry involving the source centered a distance, h, above the top of the crystal, was done as follows. The crystal was divided into two parts. One, the truncated cone formed by the top and bottom surfaces of the crystal and the locus of lines from the source to the bottom edge of the crystal, was treated as a unit which subtended a solid angle at the source that could be calculated and which had a fairly uniform thickness. The contribution of the rest of the crystal, was calculated by integrating. To permit an analytical integration, however,

the exponential absorption term was replaced by its power series of which the first four terms were sufficient for the desired accuracy (1 to 2 percent). The results of this calculation for a crystal 1.50 inches long by 1.50 inches in diameter and with h equal to 0.75 inches, is shown in Figure 5. These calculated values have been checked with a calibrated Na^{22} source and from the known yield of the $F^{19}(p,\alpha\gamma)O^{16}$ reaction. They will be used throughout the work reported here. It should be noted that the distance h is quite critical. For example, if h is changed by 0.1 inches, the efficiency is changed by approximately 8 percent.

Because of background or the presence of other gamma-rays, it is often very difficult to draw in the complete differential spectrum for a given gamma-ray. For these cases, it is advantageous to know the "efficiency" of the photo-peak. Because of the secondary processes described above, such an efficiency curve cannot be simply calculated in a manner similar to the way the total efficiency was found. It was measured, however, in the following manner. A series of curves was obtained for different energy gamma-rays (in particular, the four curves shown in Figures 2 and 3 were used), and the ratio of the area under the photo-peak to the total area under the differential pulse-height curve, was determined. The net photo-peak efficiency was found by multiplying this ratio by the computed total efficiency. The result of these measurements and cal-

culations, is shown as the lower curve in Figure 5. Besides the points obtained from the four curves shown in Figures 2 and 3, a point at 0.511 Mev was obtained by directly comparing the annihilation radiation with the 1.277 Mev radiation of Na^{22}. As is seen from Figure 5, this efficiency obeys a power law within the experimental error. Such a relationship was first pointed out to the author by R. B. Day, who also found a similar relationship using calibrated sources and a smaller crystal.

It was found that within experimental error, the ratio of the area under the photo-peak to the total area under the full curve was independent of the source-crystal geometry although very dependent on the size of the crystal. Thus, as a good approximation (there is a slight dependence of the total efficiency on geometry), this power law can be used for any source-counter geometry. Therefore, knowing the absolute photo-peak efficiency at one energy, the photo-peak efficiency at other energies can be approximately computed if the geometry is unchanged. It must be emphasized, however, that the particular exponent expressing the energy dependence depends on the size of the crystal (it becomes smaller as the crystal is made bigger).

In actual practice it is often difficult to separate the photo-peak from the background and the Compton peak. Reproducible results can be obtained, however, if the criterion is followed that the photo-peak corrected for

background be symmetrical. Such an analysis, giving the "full" photo-peak, is independent of the resolution of the counter, and such an efficiency curve as found above can be used. However, this method can be quite tedious if much data has to be handled. It has been found that just as reproducible results can be obtained by considering the front part of the Compton peak as background, and drawing in the background as shown in Figure 16. Of course, when this latter method is used, a different efficiency relationship must be found from that given above, and such a relationship is dependent on the resolution of the counter. This is because at present the resolution of the counter is such that above 1.5 Mev, the Compton peak and the photo-peak are not completely separated.

B. Experimental Techniques

One of the practical difficulties in using NaI(Tl) is that it is hydroscopic and must be protected from the air. Various methods have been used. The most satisfactory one developed in the course of this work, is shown in Figure 6. The crystal* is prepared in a dry box by cleaning all the sides with cloth and sandpaper, and leaving all the sides but the one to be cemented to the quartz disk, roughened with coarse sandpaper. Then, without removing the crystal from the dry box, it is cemented** to the quartz disk, the disk is cemented to the aluminum can, and finally the cap cemented to the can as shown in Figure 6. A diffuse reflector of MgO has been found to be better than aluminized or silvered reflectors for large crystals, and thus the inside of the aluminum can and cap are coated with Mgo. This is accomplished by holding them over burning Mg ribbon.

In placing the mounted crystal on a photo-multiplier, a Lucite matching piece and either clear mineral oil or viscous silicone oil are used to provide optical contact between the quartz disk and the photo-multiplier.

Smaller crystals (e.g., 1/2-inch cube) are conveniently handled by chemically polishing them in acetone, rinsing

---

* The NaI(Tl) crystals were obtained from Harshaw Chemical Co, Cleveland, Ohio.

** The cement used is a thermo setting type, Bonding Agent R 313, obtained from Carl H Biggs Co, Los Angeles, California.

them in water-free mineral oil, and then placing them directly on the photo-multiplier with an excess of mineral oil. A small aluminized cup is then placed over the crystal to hold it in place and to act as a reflector. Such an arrangement requires no dry box and gives satisfactory results for one or two weeks.

The most critical part of the counter is the photo-multiplier tube (RCA type 5819 was used throughout this work), for at present it is the photo-multiplier tube that determines the resolution. One of the determining factors is the uniformity of the cathode. Although diffuse reflectors are used, various parts of the cathode are illuminated differently by light originating in different parts of the crystal. Thus, if the cathode is more sensitive in some spots than in others, there will be a variation in output dependent on the place in the crystal where the primary event took place. This can be partly remedied by separating the crystal from the cathode with a Lucite light-piper. However, the loss in intensity when this is done, increases the second and more important factor which is the statistical fluctuation in the number of photo-electrons ejected from the photo-cathode. Indeed, by measuring the resolution of a counter employing a "good" photo-multiplier, one can estimate this number of photo-electrons[1]. In connection with this work, the best photo-multiplier that was used gave a resolution correspond-

ing to 7.5 percent (width at half-maximum of the photo-peak) for a 1 Mev gamma-ray. This corresponds to 1300 photo-electrons per Mev emitted from the photo-cathode. The resolution corresponding to an arbitrary energy E, is given by the familiar statistical rule

$$R_E = R_o(n_E/n_o)^{1/2} = R_o E^{1/2}$$

Here n_E is the number of photo-electrons corresponding to an energy lost in the crystal of E, n_o is the same quantity for E equal to 1 Mev, R_o is the resolution at 1 Mev, and E is in Mev. This relation holds up to about 2 Mev, above which other factors seem to predominate, and the resolution increases more slowly than predicted by statistics.

The photo-multiplier tubes are very sensitive to magnetic fields and must be shielded from them. For example, it has been found that the gain of a photo-multiplier tube may be changed by 30 percent and the resolution of the counter by 20 percent, if the unshielded counter is rotated in the earth's magnetic field. It has also been found that the maximum resolution observed for an unshielded counter is never greater than that of a shielded counter. As shown in Figure 6, a mu-metal shield is placed around the top of the photo-multiplier for shielding the earth's field and, although not necessary, the light shield is made of iron to provide extra magnetic shielding.

Since the energies of the gamma-radiation to the

ground state of N^{14} (see Part III), could be calculated from the Q-value of the reaction and the proton bombarding energies, it was possible to check the linearity of the pulse-height with energy up to 9 Mev in the counter. It was found that as long as the voltage on the photo-multiplier was kept less than about 750 volts, this linearity was good to within the experimental accuracy (1 percent). For lower energy gamma-rays, it was possible to raise the photo-multiplier voltage above 750 volts before non-linear effects were encountered.

The signal obtained from the photo-multiplier in the region of gamma-ray energies of interest here, is sufficiently high that spurious noise pulses from the photo-multiplier tube are not a problem. However, there is a type of noise known as after-pulsing[4] which is apparently caused in part by positive ion feedback and which immediately follows a true signal. The net effect of this after-pulsing is to add a tail to the signal, and the difficulties this presents will be discussed below.

The integrated current from the photo-multiplier tube with a total of 750 volts across its dynodes and for 1 Mev loss in the crystal, is of the order of a micro-micro-coulomb. The crystal has a decay time of 0.25 microseconds, and thus the integrated output pulse from the photo-multiplier tube has a similar rise time. The electronic problem is to first amplify such signals, and secondly to

analyze them with some kind of pulse-height discriminator. The following brief considerations determine the more important requirements of the amplifier. To retain the best pulse shape consistent with the original signal, the amplifier should have a rise time at least as fast as the rise time of the original signal, and preferably faster (e.g., 0.1 to 0.2 microseconds). The resolution of the counter being on the order of 10 percent, one should be able to obtain reproducible pulse-height measurements to a percent and hence the gain stability of the amplifier should be of the order of, say 0.2 percent during a series of measurements. Finally, the gain required for the amplifier, is of the order of 1000. These requirements of rise time, gain stability, and total gain are not too difficult to satisfy with a feedback-type pulse amplifier. Such amplifiers are described in Reference 5, which reference also contains a general analysis of the items mentioned here besides other pertinent considerations.

Figure 7 shows a schematic circuit of a ten-channel differential discriminator (6) that was built and used in this work. In the pre-amp, which serves as a coupling device between the photo-multiplier and the amplifier proper, the photo-multiplier current is integrated. The resulting output is essentially a step function with a rise time of 0.25 microseconds. The voltages involved at this point are so small that there is no danger of pile-up

even though the step function is made to decay with a time constant of several hundred microseconds. This step function is then shaped with a delay line clipper at the input of the amplifier to give a flat-topped pulse of the order of one microsecond wide. The after-pulsing mentioned above, however, spoils the shape of this pulse and causes it to continually rise rather than being flat. This can be corrected by slightly differentiating the signal, but this is inconvenient since each photo-multiplier acts differently in this respect.

Since the output voltages convenient to work with from the amplifier are of the order of 10 to 100 volts, the criterion of 0.2 percent stability in gain requires that the discriminators following the amplifier be stable to within approximately 0.05 volts. This is fairly difficult to accomplish even though this stability must be maintained for only several hours. To circumvent this problem, a biased or window amplifier is inserted between the amplifier and the discriminators. This is an amplifier with fixed gain which amplifies only those signals higher than some preset value. For example, suppose the gain of this amplifier is 10 and its bias is set to 40 volts. Then any signal less than 40 volts would not pass through. Signals between 40 and 50 volts would be amplified linearly from 0 to 100 volts. And signals greater than 50 volts would saturate the amplifier. This means in this particular

case that the discriminators that follow such an amplifier need only be 1/10 as stable as if they were placed directly after the amplifier. Thus, the critical point for stability is shifted from many items (the discriminators) to one item (the biased amplifier).

In the arrangement shown in Figure 7, a precision pulser was used to calibrate the discriminators and to act as a reference for actual measurements. The pulses from this pulser could be fed into the pre-amp in parallel with those from the photo-multiplier. Thus in effect, the amplifier and discriminators are used only as a comparison device between known artificial radioactive sources (such as Na^{22} and ThC" which provided the energy calibration) and the radiation under investigation. From this point of view, the only requirement on the electronics is that it be stable. In actual use, the procedure was to alternate the measurement of pulse-height from the unknown radiation with those from artificial radioactive sources. After each spectrum had been obtained, the pulse-height corresponding to peaks in the spectrum were measured with the precision pulser. Since this alternation between standard sources and the unknown gave one a check on the drifts in the photo-multiplier gain (due to drift in the high voltage across the photo-multiplier dynodes) and in the reproducibility of the electronics, one could feel confident that the gamma-ray measurements were not affected by instrumental difficulties.

It was with a discriminator like this that Figures 2, 3, and 4 were obtained.

A photographic method of analysis has also been used. After amplification, the flat-topped pulses were applied to the vertical deflection plates of a Tectronix 511 D oscilloscope with the horizontal sweep being triggered by the pulse. The face of the oscilloscope was masked except for a vertical strip 2 cm wide, and a sweep-speed of 10 cm per microsecond was used. Peaks in the pulse-height distribution then appeared as horizontal lines. A permanent record was obtained by making a time-exposure with a Land camera. The range of intensities obtainable with a single exposure, was increased by means of a colored cellophane filter placed over 1 cm of the 2 cm wide strip. To correct for non-linearities in the system, which were mainly in the oscilloscope tube and in the optical system of the camera, a series of pulses whose height could be varied in equal voltage increments were fed into the input of the pre-amp and photographed on the oscilloscope. Since five exposures could be made on each film, the general practice was to include this linearity calibration with each pulse-height spectrum of interest, in addition to the spectrum of gamma-rays of known energy which were used to establish the energy calibration. This technique proved to be very rapid and convenient, not only for qualitative "surveying" but also for quantitative results good to about 2 percent.

An example of this is shown in Figure 8 which shows Na^{22} (1.277 Mev photo-peak, the 1.277 Mev Compton peak, and the annihilation radiation photo-peak) and ThC" (2.615 Mev photo-peak, the 2.615 Mev pair-plus-one peak, the 2.615 Mev pair peak, and lower energy radiation).

The oscilloscope arrangement was also used in obtaining pulse-height spectra in gamma-gamma coincidence measurements. A second counter similar to the first was placed on the opposite side of the target from the first. Their outputs went to a coincidence circuit with a resolving time of 0.1 microseconds which was used to trigger the sweep of the oscilloscope. The output of one of the counters was applied to the vertical deflection plates of the oscilloscope, while a sufficiently high bias on the coincidence input fed by the other prevented false coincidences from back-scattered Compton gamma-rays or from annihilation radiation. Where this setup was used, the counting rates were low enough that accidental coincidences could easily be taken into account.

PART III

THE REACTION $C^{13}(p,\gamma)N^{14}$

A. Experimental Results

The thin-target excitation curve for the reaction $C^{13}(p, \gamma)N^{14}$ has previously been investigated in this laboratory for proton bombarding energies up to 2.7 Mev(7). Five definite resonances were found, corresponding to excited states of N^{14} at 8.06, 8.62, 8.70, 9.13, and 9.59 Mev. It was observed that the gamma-ray spectrum changed considerably from one resonance to another, and involved cascades through intermediate levels of N^{14}. In addition, recent work in this laboratory on the elastic scattering of protons on C^{13} has clearly demonstrated the existence of two other resonances at 1.55 Mev and 1.47 Mev(8) which were tentatively reported in Reference 7. In order to obtain more information on the energy levels of N^{14} below 9.5 Mev, the gamma-ray spectrum was investigated in detail at each of the 7 resonances using the spectrometer described in Part II.

The gamma-rays were produced by bombarding C^{13} targets with protons from the 3 Mev Van de Graaff generator of the Kellogg Radiation Laboratory. The protons were analyzed by either an electrostatic or a magnetic analyzer set to give an energy resolution of 0.1 to 0.2 percent. At each resonance, before observing the pulse-height spectrum, an

excitation curve was run in order to obtain the maximum intensity and also to be sure that the observed radiation was characteristic of the resonance. The two targets used were 7 and 16 Kev thick at 1.7 Mev, and were composed of carbon enriched to 60 percent C^{13}, deposited on a tantalum backing. The preparation of these targets is described in detail in Reference 7. The background radiation produced by reactions in the C^{12} content of the target or the tantalum backing, was investigated independently and found to be much less intense than the radiation from the reaction $C^{13}(p, \gamma)$. It could also be distinguished from the latter by its excitation function, since the resonances in $C^{13}(p, \gamma)$ are well known (7,8). In most cases the pulse-height spectra were measured with the scintillation counter placed at 90 degrees to the beam about 3/4 inch from the target. Several resonances were also investigated at 0 degrees to the beam. These results will be discussed in a later section.

Typical pulse-height distributions, which show the various features encountered at three of the resonances in $C^{13}(p, \gamma)$, are illustrated in Figures 9, 10, and 11. In Figure 9 (0.554 Mev resonance), the peaks at 1.3 and 2.3 Mev have the proper shape and separation to be the pair and photo peaks of a 2.3 Mev gamma-ray, while the rise just below 2 Mev is the Compton edge for this gamma-ray. The peak at 1.6 Mev is the photo peak of a 1.6 Mev gamma-ray

whose Compton edge is obscured by the 1.3 Mev pair-peak. The rise below 1.3 Mev is the tail of the annihilation radiation from the positron decay of N^{13} which is formed in the reaction $C^{12}(p,\gamma)N^{13}$. A similar pulse spectrum occurred also at the 1.16 Mev resonance, which suggests that the 1.6 and 2.3 Mev gamma-rays are part of a cascade through the lower levels of N^{14}. In the region of pulse-heights from 3 - 4 Mev in Figure 9, there occur three peaks characteristic of a 4 Mev gamma-ray. The peak at 7 Mev in Figure 9 is produced by an 8 Mev gamma-ray. Its structure is caused by contributions from the high-energy end of the Compton distribution in addition to the secondary effects mentioned in Part II.

The possibility of weak resonant radiation in the 5 to 7 Mev region was easily checked by using the photographic method. By stopping the camera down and taking long runs in such situations as this, one is able to "statistically smooth out" the background and observe any real "bumps" that would correspond to gamma-radiation. Besides using the photographic technique for better statistics, there is, in addition, no fear of erroneous lines appearing because of uneven or varying "channel widths" as with an electronic analyzer.

The radiation at the 0.554 Mev resonance was intense enough to permit a gamma-gamma coincidence experiment to be performed using the photographic technique to record the

pulse-height distribution. This experiment showed that the 4 Mev gamma-ray plus the 2.3 and 1.6 Mev gamma-rays were related in some sort of cascade transition.

At the 1.16 Mev resonance, in addition to the 1.6 and 2.3 Mev gamma-rays, there appeared in the pulse-height distribution a complicated structure in the 4 Mev region which was resolved into two gamma-rays at 4 and 4.7 Mev respectively. Also present were a 6.2 Mev gamma-ray and some ground-state radiation (8.62 Mev). From energy considerations, it is obvious that the 4 and 4.7 Mev gamma-rays form one cascade. The 1.6, 2.3, and 4.7 Mev gamma-rays form another. And the 2.3 and 6.2 Mev gamma-rays form a third. The fact that only one 4 Mev gamma-ray was found at the 0.554 Mev resonance can easily be explained if a level is assumed to be at 4 Mev in N^{14} since the radiation from the excited level (8.06 Mev) at this lower resonance to such a level could not be separated from the ground-state decay of such a level. The measured yields confirm this scheme.

The 1.25 Mev resonance emits mostly ground-state radiation. This and the fact that the resonance was very weak, prohibited a detailed investigation of the cascading with the ten channel discriminator. However, the photographic method revealed a complicated spectrum that is believed may involve a level in N^{14} at 5.69 Mev. This possibility will be discussed later.

To measure the energy of a particular gamma-ray, the pulse-height spectrum in question is looked at in detail on an expanded scale, and compared with a standard source as described in Part II. To eliminate systematic errors due to possible differences in channel widths in using the ten-channel analyzer, the bias settings are chosen to give over-lapping intervals. An example of this is shown in Figure 10 where the 2 to 3.5 Mev region of the spectrum from the 1.47 resonance is shown. This very complicated spectrum is explained as follows. The 2.08, 2.57, and 3.09 Mev peaks are the three characteristic peaks of a 3.09 Mev gamma-ray. The 2.33 and 2.76 peaks are the photo-peaks for two weaker gamma-rays of approximately these measured peak values. There is no question about the 2.33 peak being a photo-peak but since the 2.76 peak coincides with the Compton maximum from the 3.09 Mev gamma-ray, it may be in doubt. However, the pronounced dip between the 2.76 peak and the 2.57 peak, and the general rise in counting rate indicates that there is indeed a gamma-ray present of approximately this energy. The rather flattened appearance of the ThC" line (2.615 Mev photo-peak) and the 3.09 peak, is because the channel width used (1 volt) is comparable to the resolution at this particular setting. Besides these gamma-rays, three others at 5.7, 5.1, and 0.73 Mev were also found at this resonance. Since the 3.09 gamma-ray was the strongest, it most likely is the first in the cascade. If this is assumed, then one

calculates that there is a level at 5.81 Mev (8.90 minus 3.09) in N^{14}. Energy considerations then indicate that the 5.1 and the 0.73 Mev gamma-rays result from the decay of this 5.81 level, and the 2.3 and 2.8 Mev gamma-rays result from an alternative decay of the 5.1 level. This scheme is further confirmed by the spectrum from the 2.1 Mev resonance and from the relative intensities.

The 1.55 Mev resonance yields mostly ground-state radiation. Because it was so weak and superimposed on the broad 1.25 Mev resonance, any cascading less than 15 percent of the ground-state radiation could not have been detected.

The radiation at the 1.76 Mev resonance is almost wholly to the ground-state of N^{14}. There is, however, a weak cascade consisting of a 6.5 and a 2.73 Mev gamma-ray. A coincidence measurement showed that these two were indeed in cascade as can be deduced from the fact that their energies add up to the full energy available.

Gamma-rays from the 2.1 Mev resonance (Figure 11) were found at energies of 2.3, 2.8, 4.4, and 5.1 Mev. The radiation above 5.1 Mev did not show resonance and is believed to be from fluorine contamination in the Ta used as a target-backing. Energy considerations indicate that there are two cascades, one consisting of the 4.4 and 5.1 Mev gamma-rays and the other consisting of the 2.3, 2.8, and 4.4 Mev gamma-rays. The relative intensities are consistent with this interpretation.

This data is summarized in Table I while the proposed decay schemes are shown in Figure 12. In Table I, the best values for the energies of these transitions are listed for comparison with our observed values. They were obtained as follows. The three lowest values and the 3.95 value are from the beta-ray spectrograph analysis of the gamma-radiation from C^{13} plus H^2 (9). The 6.44 and 5.81 values are obtained by subtracting the energy obtained for the softer cascade gamma-ray from the calculated Q-values of the corresponding resonance involved. The 5.08 value is obtained by subtracting 0.725 (9) from 5.81, and the rest are obtained by taking differences between these energies (see the decay schemes in Figure 12).

The relative intensities listed for the decay schemes were obtained by measuring the area under the pulse-height curve or under the photo-peak as described in Part II.

Since the 8.06 and 8.70 Mev resonance levels are formed by s-wave protons (7, 10), any radiation resulting from the decay of these levels will be isotropic and the measured intensity ratios are identical with the ratios obtained by integrating over the whole sphere. Of the other resonance levels, only the relative intensity of the decay of the 9.17 Mev level has been corrected for the angular anisotropy of the radiation. However, the expected maximum anisotropy in each of the other cases would not cause more than a 20 percent change in the measured value, and in most cases the

TABLE I Gamma-radiation From $C^{13}(p,\gamma)N^{14}$ (All energies in Mev)

E_R	0.554	1.16	1.25	1.47	1.55	1.76	2.10	Best Values
E_X	8.06	8.62	8.70	8.90	8.98	9.17	9.49	
MEASURED GAMMA-RADIATION	8.03±.10	8.6±.1	8.7±.1		9.0±.1	9.17±.10		
						6.5±.1		6.44±.02
		6.2±.1						6.31±.02
				5.7±.2				5.81±.02
				5.1±.1			5.09±.05	5.08±.02
		4.7±.2						4.68±.02
							4.41±.08	4.36±.02
	4.0±.1	3.94±.06						3.95±.02
			(3.9)?	3.09±.02				
			(3.4)?					
				2.8±.1			2.78±.04	2.77±.03
			(3.0)?					
						2.73±.02		
	2.32±.02	2.35±.04	2.3	2.32±.04			2.32±.02	2.310±.012
	1.63±.02	1.66±.02						1.638±.008
				.731±.007			(.73)?	.725±.004

difference is probably much less than the experimental error.

The resonance characteristics for the seven resonances investigated are listed in Table II. With the exception of the 1.47 and 1.55 Mev resonances and the recalculated reduced widths, the table is essentially Table III in Reference 7. The dimensionless reduced width, $\theta^2 = \gamma^2(\hbar^2/2Ma)^{-1}$, where γ^2 is the reduced level width of Wigner and Eisenbud[11], has been calculated employing the coulomb tables of Bloch et al[12], with an interaction radius of $1.41(13^{1/3} + 1)10^{-13}$ cm. The quantity $1/\theta^2$ may be interpreted as the number of nuclear traversals of the incident particle in the compound system. Wigner's criterion[13] places an upper limit on θ^2 of 3, and with this condition one is able to place an upper limit on the possible ℓ value of the incident particle. In these calculations, the variation of level shift with respect to energy[14] has been taken into account which correction has little effect on values of θ^2 less than one, but tends to increase those values greater than one. Thus the correction may be important in clearly establishing which partial waves are permitted and which are not. At all but the 0.554 and 1.25 Mev resonances, a WKB approximation was used in calculating this level shift correction which resulted in an over-correction and hence the infinities in the table.

TABLE II Resonance Characteristics for $C^{13}(p,\gamma)N^{14}$

E_R (Mev)	Γ_p (Kev)	Θ^2 s-wave	p-wave	d-wave	f-wave	g-wave	σ_R (10^{-3} b)	$\omega\Gamma_\gamma$ (ev)
0.55	32.5±1	.4	13				1.44	8.6
1.16	6 ± 2		.04	.3	∞		0.56	1.3
1.25	500	.7	4.5				.062	12.8
1.47	20		.05	.5	∞		.074	.71
1.55	7		.016	.1	4		.037	.13
1.76	2.1±.2			.024	.4	∞	12.0	14.8
2.10	45 ± 3		.05	.3	∞		1.96	6.15

TABLE III Angular Anisotropy of Four Gamma-rays from $C^{13}(p,\gamma)N^{14}$

E_R (Mev)	Transition in N^{14*} (Mev)	Anisotropy Ratio a
1.47	8.90 → 5.81	+0.25 ± 0.10
1.76	9.17 → gnd state	-0.48 ± 0.03
1.76	9.17 → 6.44	-0.05 ± 0.10
2.1	9.49 → 5.08	+0.48 ± 0.15

However, from these calculations this approximation seems to be valid in the region of interest (θ^2 of the order of 3).

From these calculations and Wigner's criterion, it is seen that the 0.554 and 1.25 Mev resonances are formed by s-wave protons and that all the rest, with the exception of the 1.76 Mev resonance and possibly the 1.55 Mev resonance, are formed by partial waves with $\ell \geq 2$.

Table II also gives the total gamma-ray width Γ_γ times the statistical factor ω for each of the seven resonances. In this reaction, $\omega = (2J + 1)/4$ where $\hbar J$ is the total angular momentum of the compound state.

In an attempt to determine the angular momenta of some of the levels involved in the cascading, the anisotropy ratio, a = yield(0^o)/yield(90^o)-1 was measured for the first gamma-ray in the cascades found at the 1.47, 1.76, and the 2.1 Mev resonances. Also, the angular distribution of the ground-state transition at the 1.76 Mev resonances was measured and the results for this latter measurement are in excellent agreement with previous measurements[15]. The anisotropy ratios for these four cases are listed in Table III.

B. The Energy Levels of N^{14}

An energy level diagram of N^{14} showing the known levels up to 10 Mev and including the results described above, is shown in Figure 13. Of the many experiments that are given in the review article of F. Ajzenberg and T. Lauritsen(16) yielding information about the levels shown here, two will be discussed as they apply directly to this work. The first of these is the thin-lens spectrometer analysis of the gamma-radiation from $C^{13}(d,n\gamma)N^{14}$ (9). Although Thomas and Lauritsen do not report a ground-state transition from the 3.95 Mev level, further work under improved conditions has apparently revealed it(17) in agreement with what was found in this work. Thomas and Lauritsen also report a 3.38 Mev gamma-ray which they assign to N^{14} in cascade with the 2.31 Mev gamma-ray. Coincidence measurements with two scintillation counters on the $C^{13}(d,n\gamma)N^{14}$ reaction has confirmed this assignment.* This, then, places a level at 5.69 Mev in N^{14} as shown in Figure 13. Thomas and Lauritsen also report a 5.69 Mev gamma-ray which they believed to be the ground-state transition of this level. It is believed that the weak low energy radiation found at the broad 1.25 Mev resonance described before, may involve this level. It is noted that this resonance is the only resonance of

---

* The coincidence measurements reported here, were made by J Thirion for the author.

the seven investigated, that indicated a 3.4 Mev radiation.

As noted before, Thomas and Lauritsen found a strong 0.725 Mev gamma-ray which is believed to correspond to the 0.73 Mev gamma-ray found at the 1.47 Mev resonance. In the following discussion, these two gamma-rays will be assumed to be the same. Coincidence measurements, again on the $C^{13}(d, n\gamma)N^{14}$ reaction, have shown that this 0.725 Mev radiation is in cascade with radiation above 4.5 Mev and below 5.2 Mev which disproves the suggestion that the 0.725 Mev radiation was the result of a transition between the 4.8 Mev level and the 3.95 Mev level[16]. Thus, the possible levels from which the 0.725 Mev gamma-ray can originate, are a tentative level reported at 5.5 Mev[18], the level at 5.69 Mev, and the one indicated by these experiments at 5.81 Mev. The first two possibilities would presumably decay to the 4.8 Mev level, while the latter goes to the 5.08 Mev level. The energy measurements of the cascading gamma-rays associated with the 0.725 Mev gamma-ray, preclude any such level as low as 5.5 Mev. The 5.69 Mev level cannot be associated with the 0.725 Mev radiation since at the resonance the 0.725 Mev gamma-ray was found, there was no indication of the 3.38 Mev gamma-ray (see Figure 10) which results from the decay of the 5.69 Mev level. Thus the 0.725 Mev gamma-ray appears to certainly come from the 5.81 Mev level as postulated. However, this would mean that Thomas and Lauritsen should have found a

5.81 Mev radiation one-third as intense as the 0.725 Mev radiation. This they did not do, and as yet there is no explanation of the discrepancy.

The second piece of work to be noted, is the recent neutron work of Benenson[18] who has confirmed the assignment of the level at 6.44 Mev.

From the anisotropy measurements and the reduced widths, few unambiguous conclusions can be drawn. However, limits on the angular momentum of some of the levels can be given. Consider first the 2.1 Mev resonance (the 9.49 Mev level in N^{14}). Since the radiation from this level is not isotropic (Table III) it cannot be formed by s-wave protons nor can it have an angular momentum of 0. Thus, since the reduced width (Table II) indicates that the level can only be formed by partial waves with $\ell \leq 2$, the angular momentum of the level must be 1^+, 2^+ (p-wave protons) or 2^-, 3^- (d-wave protons). (Here and below the angular momentum will be given in units of $\hbar$). <u>If</u> the radiation resulting from the transition between this level and the 5.08 Mev level is pure dipole (this radiation has an energy of 4.4 Mev and a width, ω/γ , of 6 ev), then the measured anisotropy ratio precludes the possibility of 3^- for the angular momentum. Also, under this assumption of pure dipole radiation, the 5.08 Mev level must have the same angular momentum as the 0.49 Mev level (1 or 2).

The 9.17 Mev level has been given a tentative angular

momentum assignment of 2 (15). If this is the case and if the transition to the 6.44 Mev level gives pure dipole radiation (this radiation has an energy of 2.7 Mev and a width, $\omega\Gamma_\gamma$, of 1.5 ev), then the 6.44 Mev level has an angular momentum of 3.

The elastic scattering of protons by C^{13} and the reduced width indicate that the 8.90 Mev level in N^{14} is formed by d-wave protons giving an angular momentum and parity of 2^- or 3^- with the second value being preferred(8). The transition between the 8.90 Mev level and the 5.81 Mev level gives 3.1 Mev radiation and has a width, $\omega\Gamma_\gamma$, of 0.7 ev. If this radiation is pure dipole, then the anisotropy ratio agrees best with the 2^- assignment and furthermore requires that the 5.81 Mev level have an angular momentum of 2. Actually, the agreement is not good. With 100 percent channel spin 1 (the most favorable case), the calculated anisotropy ratio is 0.42 which is to be compared with the experimental value of 0.25 ± 0.10. If, on the other hand, the radiation is pure quadrupole, then the 3^- assignment is permissible only if the 5.81 Mev level has an angular momentum of 5 which value, however, appears improbable from the decay schemes. In the actual situation, as also in the other cases considered above, there may be involved a mixture of dipole and quadrupole radiation, in which case these arguments are invalidated.

Again, the elastic scattering of protons by C^{13}

indicates that the 8.62 Mev level is formed by p-wave protons and that it has a low angular momentum (0 or 1)[8]. Therefore, if the assignment of a transition from this level to the 2.31 Mev level (known to have zero angular momentum[16]) is correct, then the 8.62 Mev level must be 1^+.

Further work to determine the angular distributions of the many gamma-rays found at these several resonances, promises to be a fruitful method for uniquely determining the angular momentum of the levels and the types of radiation involved in N^{14}. Until such time, however, little can be said about selection rules and transition probabilities.

PART IV

THE REACTION $C^{12}(p,\gamma\, p')C^{12}$

A. Experimental Problems and Results

While looking for low energy radiation in the $C^{13}(p,\gamma)$ experiment, a very weak gamma-ray was found which varied in energy with the proton bombarding energy. This radiation was demonstrated to come from the C^{12} content of the target (the targets were 40% C^{12} and 60% C^{13}) when a proportionally increased yield was obtained with a normal carbon target. A linear energy dependence with respect to bombarding energy was first established, and is shown in Figure 14. A least squares fit to these points, gives

$$E_\gamma = 0.88(E_p - 0.45)$$

where E_γ and E_p are in Mev. Since no other gamma-rays with a similar energy dependence were found, the following mechanism was suggested. The proton is "captured" by the C^{12} forming a system which radiates to the well known level in N^{13} at 2.369 Mev[16] (see Figure 15). However, since this level is in the continuum, it decays by breaking up into the proton and C^{12} rather than by emission of a second gamma-ray to the ground-state of N^{13}. The gamma-ray energy of such a reaction would be given by

$$E_\gamma = 12/13(E_p - 0.456) = 0.92(E_p - 0.456)$$

where E_γ and E_p are again in Mev. The coefficient 12/13

is the reduced mass factor while the term 0.456 Mev is the observed proton capture resonance energy for the formation of the 2.369 Mev level. The observed energy dependence agrees with this within experimental error. Further work, described below, has proven this suggested process to be correct.

The next experimental problem was to find the excitation curve for this reaction. The gamma-ray was so weak, however, that it could only be detected by observing the characteristic photo-peak produced in the counter by the radiation. (The gamma-ray energies involved here, range from 0.6 to 2 Mev). Thus, the yield measurements consisted of taking differential pulse-height spectrums of the radiation at various bombarding energies, and then integrating the area under the photo-peak after making a systematic correction for the background as discussed in Part II. Three examples of such pulse-height distributions are shown in Figure 16.

Two types of targets were used, one of which was prepared by holding cleaned tantalum over a smoky benzene flame. A second type was prepared by cracking methane (natural gas) on cleaned tantalum, similar to the preparation of the C^{13} targets(7).

It was found that the targets were easily contaminated, either by handling or by simply leaving them uncovered in the laboratory. This contamination resulted in a 1.65 Mev

gamma-ray from the known prolific reaction, $Na^{23}(p,\alpha\gamma)Ne^{20}$ (16). Although the intensity of such radiation was usually small compared to other background, the fact that its energy is similar to the energy of the radiation of interest when bombarding with 2.2 Mev protons meant that the photo-peak that was sought was spoiled by the photo-peak resulting from this sodium contamination. To check against this and other possible contaminants, differential pulse-height curves were often taken up to pulse-heights corresponding to 3 or 4 Mev to make sure that there was no structure except for the smoothly varying background.

A second contaminant was believed to be F^{19} in the tantalum used for a target backing. Because the characteristic 6 and 7 Mev radiation from the $F^{19}(p,\alpha\gamma)O^{16}$ reaction gives no structure in the region of pulse-heights of interest, this contaminant was not a problem below 2.2 Mev bombarding energy. However, above 2.5 Mev, the yield from this reaction so increased that it proved troublesome.

There was also "background" from the known proton capture reactions in C^{12} and C^{13} which, since it gave for the most part higher energy radiation, did not prove too difficult to cope with. However, the annihilation radiation of the positrons coming from the decay of the N^{13} formed in the target, made it impossible to observe radiation below about 0.6 Mev.

The target thickness was found by taking an excitation

curve of the 1.76 Mev resonance of C^{13} which resonance is strong enough to be observable in natural carbon. Since this resonance has a width of only 2 Kev and the targets that were used were 20 to 100 Kev thick for 1.76 Mev protons, the observed resonance width was essentially the target thickness.

The proton currents normally used were between 3 and 5 microamperes with the maximum value being limited by the heating of the target. This current was measured by collecting it on a 10 micro-farad capacitor in connection with the usual type of integrating circuit. Even though this large capacitor was used, the integrator was often cycled as much as 6 times per run (corresponding to approximately 0.003 coulombs). A constant current source of known magnitude was used to calibrate the integrator and to measure the soakage effects in the capacitor when it was cycled.

Corrections for absorption in the target chamber ranged between 2 and 4 percent while corrections for absorption in the target-backing (when the zero degree measurements were made), amounted to approximately 20 percent. The cross-sections for these corrections were obtained from Reference 2.

The normalization between the data taken with the counter at 90^{o} and at 0^{o} with respect to the beam, was made in various ways. One was to attempt to duplicate the target-

counter geometry in each case with a Na^{22} source of known strength, while another and more satisfactory method was to compare the yield of the isotropic proton capture radiation from the 0.456 Mev resonance in C^{12} (19).

Using the procedure outlined in Part II, the efficiency for producing the photo-peak was found, and with the absorption corrections mentioned above, the total effective isotropic yield, Y, was found. The cross-section was then calculated using the relation

$$\frac{d\sigma(E)}{d\Omega} = Y \cdot \frac{\Delta E}{4\pi \epsilon(E)}$$

where ΔE is the target thickness, $\epsilon(E)$ is the stopping power of carbon as given by Hirschfelder and Magee (20), and E, the effective or average bombarding energy, is given by $E = E_p - \Delta E/2$. The results of these measurements and calculations, are shown in Figure 17.

B. Descriptive Theory of the Reaction $C^{12}(p,\gamma p')C^{12}$

The excitation curves shown in Figure 17, indicate that the radiation is of two parts which interfere at proton energies around 1.7 Mev. One part is clearly a resonant radiation at 1.7 Mev, while the other is a non-resonant radiation which has a $\sin^2\theta$ form of angular distribution. (The observed off-resonance radiation at 0^o is due to the finite solid angle of the counter. See below). Consider first the non-resonant radiation. It is impossible to account for the lack of radiation at 0^o by assuming the formation of a compound state. Also, the excitation curves indicate that no ordinary resonant compound state is formed. Professor Christy has suggested that the explanation lies in a no-spin flip process of radiative capture which, for this reaction, can be described as follows. Consider ℓ wave protons incident on C^{12}. The intrinsic spin or angular momentum of the C^{12} is zero, and that of the proton is 1/2 in units of $\hbar$. The z-axis is defined as the direction of the proton beam, and hence the z-component of the orbital angular momentum of the proton is zero. Thus, the z-component of the total spin of the C^{12} plus proton system is given by the intrinsic spin of the proton, and may be either 1/2 or -1/2 with equal probability. The level to which the gamma-ray transition takes place (the 2.369 Mev level in N^{13}), is known to be formed

by s-wave protons[19], and hence has a spin of 1/2 with again a z-component of either 1/2 or -1/2. In a no-spin flip process, this z-component is not changed, i.e., no compound system is formed in which the projection of the angular momentum is changed. Thus, the gamma-radiation that is emitted carries away ℓ units of angular momentum (just the orbital angular momentum of the incident protons) which momentum has no z-component. Since the angular distribution of the radiation is determined only by the total angular momentum it carries away and by the component of that angular momentum on the reference axis, the angular distribution is completely determined in this case. For odd ℓ, the distribution is zero at 0° and 180° and in particular, for ℓ equal to one (corresponding to p-wave protons and electric dipole radiation) the distribution is just $\sin^2\theta$. In the discussion below, only p-wave protons will be considered as contributing to this radiation. It is noted that s-wave protons do not enter into the process since they cannot give rise to radiation when dropping into an s-state. In brief, this process may be described as the radiative capture of p-wave protons into an s-state.

At a proton bombarding energy of 1.7 Mev, there is a p-wave resonance[19] (see Figure 15) that should also radiate to the 2.369 Mev level with electric dipole radiation and which would, therefore, interfere coherently with the non-resonant radiation. Taking this into account,

the relative intensity of the gamma-radiation is given by

$$\left| \frac{(2/3)^{1/2} A \Gamma/2 \, e^{i\delta}}{\Delta E + i \Gamma/2} + 1 \right|^2 \sin^2\theta + \left| \frac{(1/3)^{1/2} A \Gamma/2 \, e^{i\delta}}{\Delta E + i \Gamma/2} \right|^2 \frac{(1+\cos^2\theta)}{2} .$$

The first term represents the no-spin flip process giving a $\sin^2\theta$ angular distribution. The resonant part of the radiation is characterized by the amplitude A (which is to be compared with the amplitude of the non-resonant radiation taken arbitrarily as a constant equal to 1), the width Γ, and an arbitrary phase shift between the resonant and non-resonant radiations of δ . The quantity Δ E is the difference between the bombarding energy and the resonance energy. The factor $(2/3)^{\frac{1}{2}}$ in this first term is a Clebsch-Gordan coefficient(21) whose square gives, in this case, the relative probability that the no-spin flip process occurs for the resonant reaction.

The second term in the intensity expression gives the contribution of the resonant radiation in which the spin is flipped or, in other words, the z-component of the angular momentum carried away by the radiation, is one unit. This situation gives an angular distribution of the form $(1 + \cos^2\theta)$. The factor $(1/3)^{\frac{1}{2}}$ is again a Clebsch-Gordan coefficient whose square gives the probability for the occurrence of this second case in which the spin is flipped.

This intensity expression becomes, when expanded,

$$\sin^2\theta + \frac{5/24\, A^2\Gamma^2 - 1/8\, A^2\Gamma^2\cos^2\theta + \left[(2/3)^{1/2} A\Gamma\Delta E\cos\delta + (1/6)^{1/2} A\Gamma^2\sin\delta\right]\sin^2\theta}{4E^2 + \Gamma^2/4}$$

and far from resonance, this is seen to reduce to just $\sin^2\theta$ as was predicted above for the non-resonant radiation. For θ equal to 90°, the expression takes the form

$$1 + \frac{5/24\, A^2\Gamma^2 + (2/3)^{1/2} A\Gamma\Delta E\cos\delta + (1/6)^{1/2} A\Gamma^2\sin\delta}{\Delta E^2 + \Gamma^2/4}$$

This expression has been plotted in Figure 17 with the exception that the non-resonant radiation is assumed to follow the dashed line shown, rather than be constant. In the calculations, the width of the 3.511 Mev level in N^{13} is taken to be 60 Kev and the proton resonant energy to be 1.70 Mev[19]. The values of the other two constants were chosen to give the best looking fit to the data. The results obtained are

$$\delta = 56^\circ + 180^\circ$$
$$A = 1.62$$

or

$$\delta = 34^\circ + 180^\circ$$
$$A = 1.11.$$

Both pairs of values give identical results for Θ equal to 90°, and they give a "symmetrical" expression which algebraically looks like

$$1 + \frac{0.75\Gamma\Delta E}{\Delta E^2 + \Gamma^2/4} .$$

For Θ equal to 0°, the original expression reduces to just

$$\frac{1/2\, A^2\Gamma^2}{\Delta E^2 + \Gamma^2/4}$$

and thus the zero degree data permits the determination of the correct set of the values found at 90°. It has been found that the second pair,

$$\delta = 34^{\circ} + 180^{\circ}$$
$$A = 1.11$$

agrees best with the data. What has been actually plotted in Figure 17 for Θ equal to 0°, is the value of the intensity for the above values of A and δ, and with Θ equal to 20°. This value of Θ is representative of the effective counter angle that the target sees.

An attempt was made to find radiation that would correspond to radiative capture of s-wave protons into the 3.511 Mev p-state in N^{13}. Because of the higher bombarding energy required, the conditions were not too favorable, and the attempt failed to show any such radiation as strong as the p-wave capture radiation. Proton energies up to 2.7 Mev were used.

REFERENCES

1. R Hofstadter and J A McIntyre, Phys Rev 79, 389 (1950)

2. Davisson and Evans, Rev Mod Phys 24, 79 (1952)

3. J G Campbell and A J F Boyle, Australian Jour of Phys Vol 6, No 2 (1953) (To be published)

4. D W Mueller et al, Nucleonics Vol 10, No 6, 53 (1952)

5. Elmore and Sands, Experimental Electronics, McGraw-Hill (1950)

6. C W Johnstone, Nucleonics Vol 11, No 1, 36 (1953)

7. John D Seagrave, Phys Rev 85, 197 (1952)

8. E A Milne, PhD Thesis, Calif Institute of Tech (1953)

9. R G Thomas and T Lauritsen, Phys Rev 88, 969 (1952)

10. Devons and Hine, Proc Roy Soc (London) 199, 56, 73 (1952)

11. Wigner and Eisenbud, Phys Rev 72, 29 (1947)

12. I Bloch et al, Rev Mod Phys 23, 147 (1951)

13. E P Wigner, Amer Jour of Phys 17, 99 (1949)

14. R G Thomas, Phys Rev 81 148 (1951) and Private Communication

15. R B Day, PhD Thesis, Calif Institute of Tech (1951)

16. F Ajzenberg and T Lauritsen, Rev Mod Phys 24, 321 (1952)

17. Robert J Mackin, Private Communication

18. Benenson, Phys Rev 87, 207A (1952) and Private Communication

19. Jackson and Galonsky, Phys Rev 89, 370 (1953)

20. Hirschfelder and Magee, Phys Rev 73, 207 (1948)

21. B L van der Waerden, Die Gruppentheoretische Methode In Der Quantenmechanik, (Edwards Brother, Inc, Ann Arbor, 1944) page 68

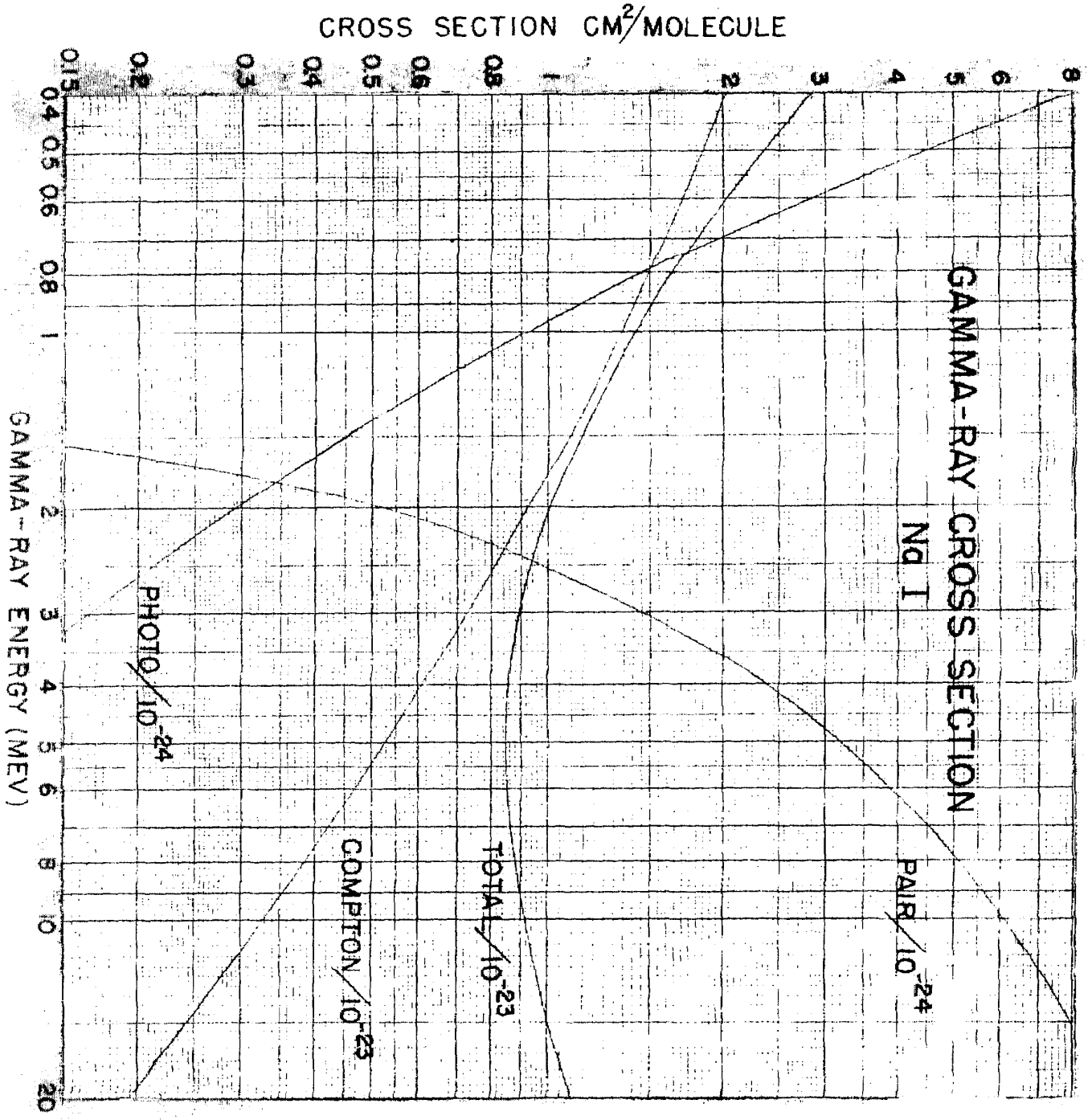
CROSS SECTION CM²/MOLECULE
GAMMA-RAY CROSS SECTION
Na I
GAMMA-RAY ENERGY (MEV)
PHOTO/10⁻²⁴
COMPTON/10⁻²³
TOTAL/10⁻²³
PAIR/10⁻²⁴

Figure 1

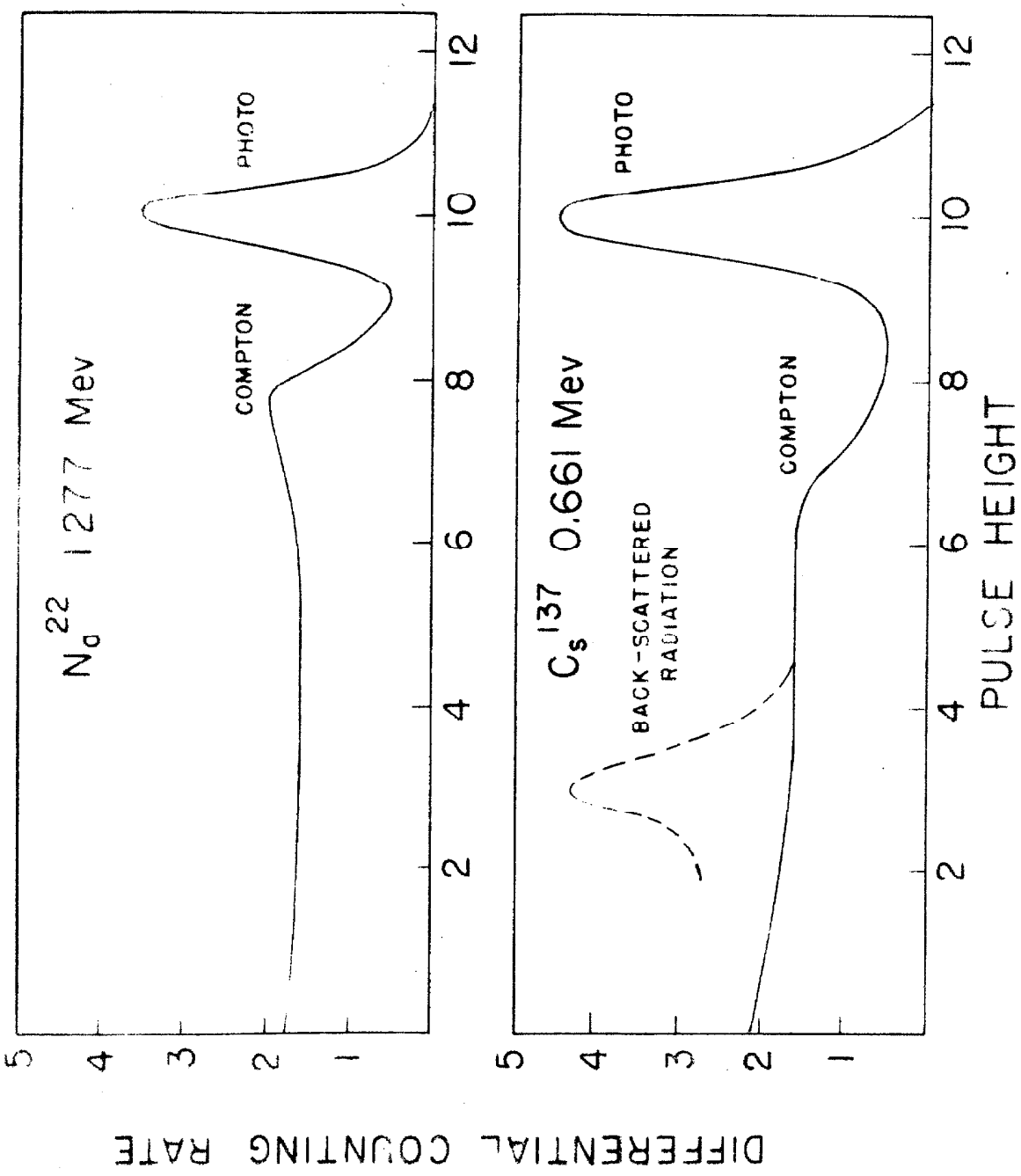
N_a^{22} 1277 Mev
PHOTO
COMPTON
C_s^{137} 0.661 Mev
PHOTO
COMPTON
BACK-SCATTERED RADIATION
DIFFERENTIAL COUNTING RATE
PULSE HEIGHT
1
2
3
4
5
2
4
6
8
10
12

FIGURE 2

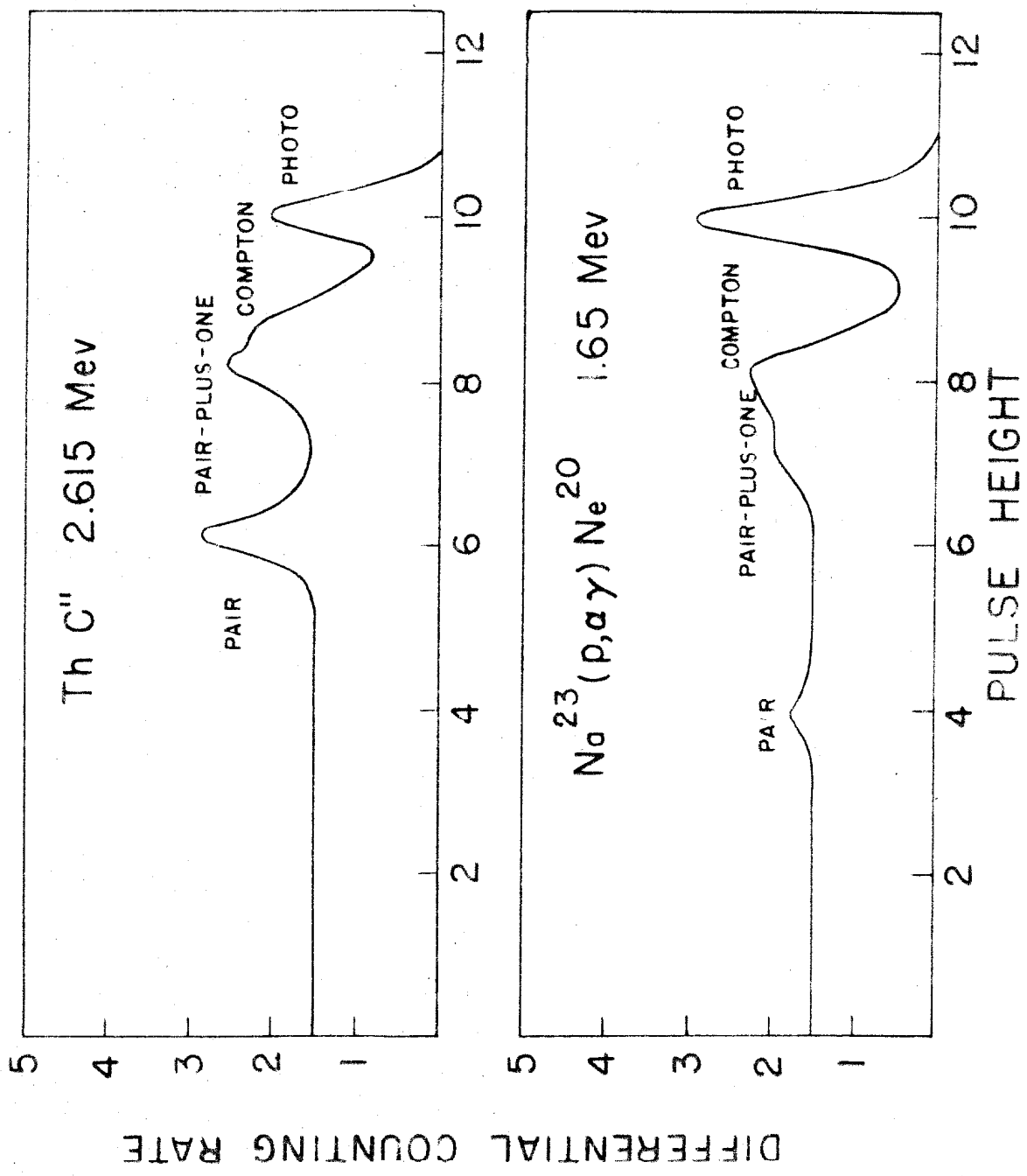
Th C'' 2.615 Mev
PAIR
PAIR-PLUS-ONE
COMPTON
PHOTO
$Na^{23}(p,\alpha\gamma)Ne^{20}$ 1.65 Mev
PAIR
PAIR-PLUS-ONE
COMPTON
PHOTO
DIFFERENTIAL COUNTING RATE
PULSE HEIGHT
1
2
3
4
5
2
4
6
8
10
12

FIGURE 3

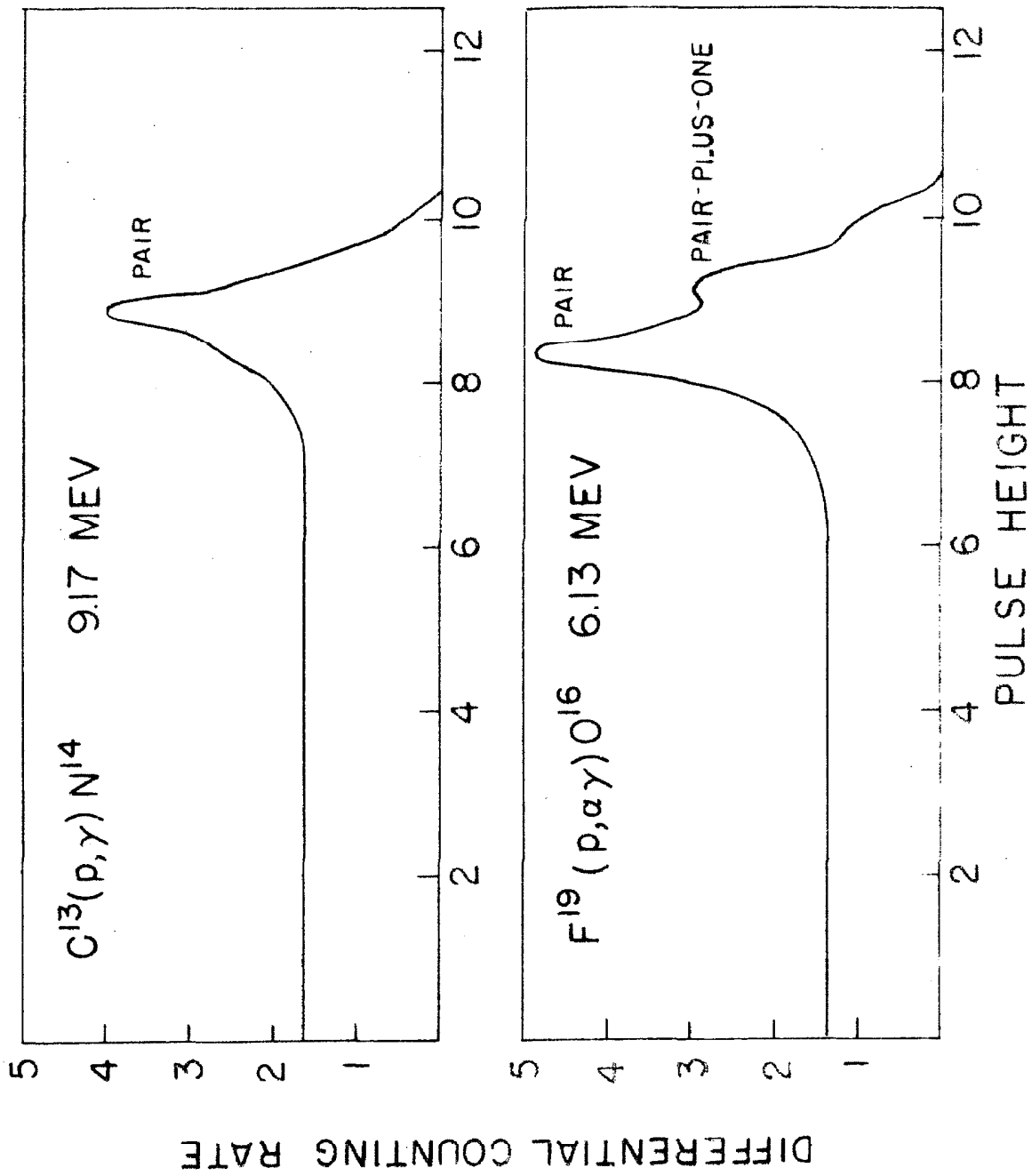
$C^{13}(p,\gamma)N^{14}$ 9.17 MEV
PAIR
$F^{19}(p,\alpha\gamma)O^{16}$ 6.13 MEV
PAIR
PAIR-PLUS-ONE
DIFFERENTIAL COUNTING RATE
PULSE HEIGHT
1
2
3
4
5
2
4
6
8
10
12

FIGURE 4

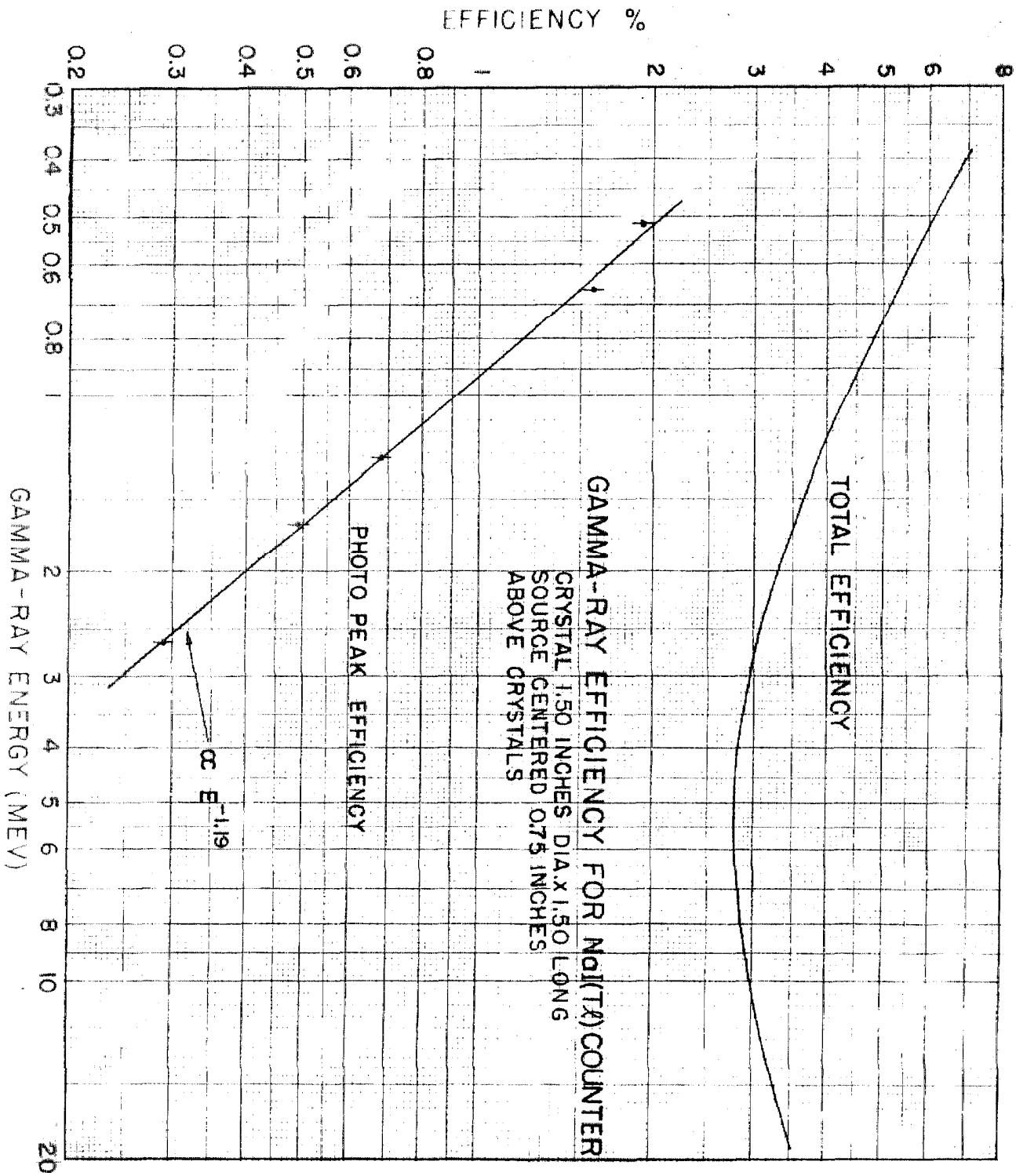
EFFICIENCY %
GAMMA-RAY ENERGY (MEV)
GAMMA-RAY EFFICIENCY FOR NaI(Tℓ) COUNTER
CRYSTAL 1.50 INCHES DIA. x 1.50 LONG
SOURCE CENTERED 0.75 INCHES
ABOVE CRYSTALS
TOTAL EFFICIENCY
PHOTO PEAK EFFICIENCY
α E^-1.19

Figure 5

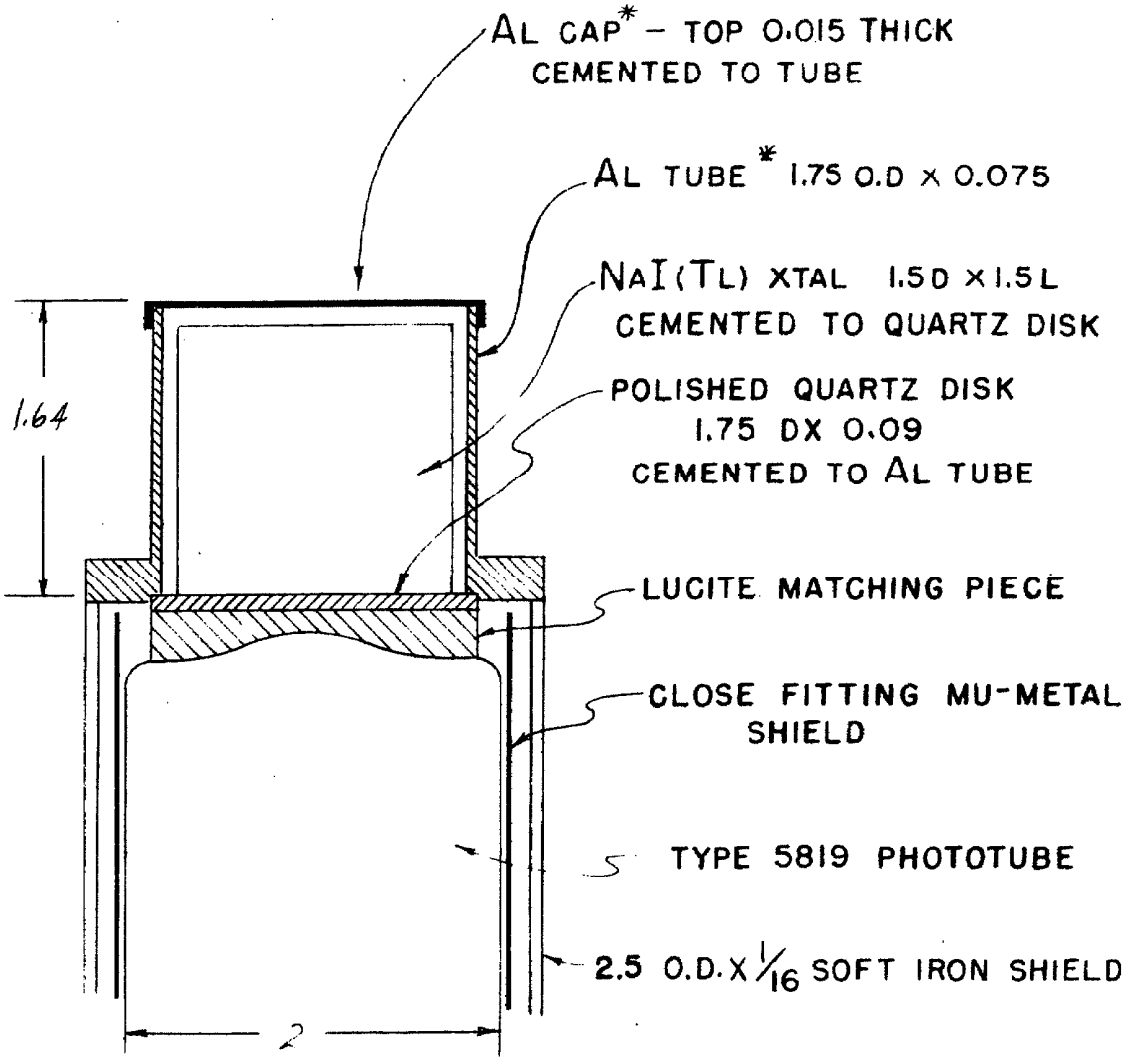

* INSIDE OF AL CAP AND AL TUBE
COATED WITH MgO

ALL DIMENSIONS IN INCHES

FIGURE 6

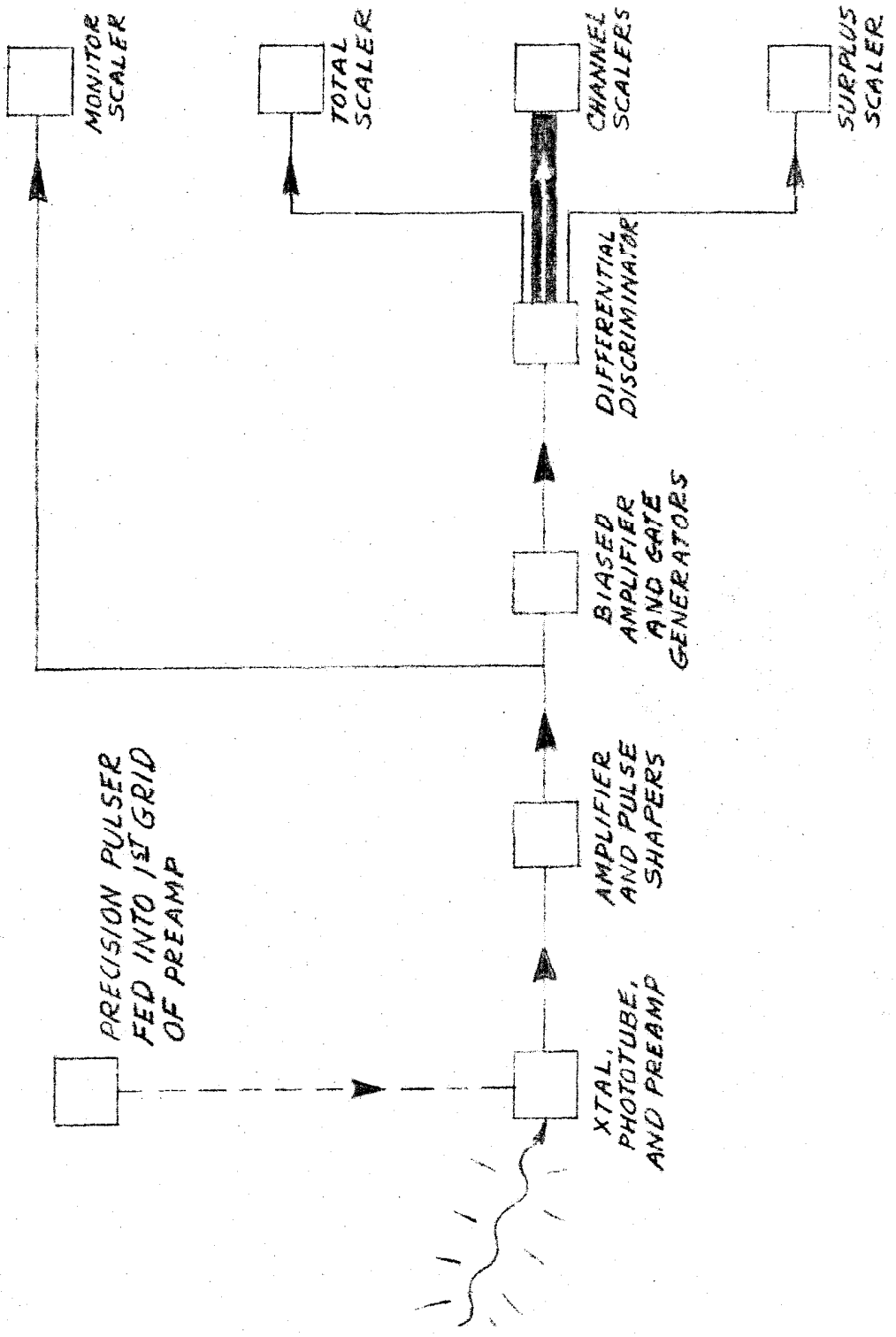
MONITOR SCALER
TOTAL SCALER
CHANNEL SCALERS
SURPLUS SCALER
DIFFERENTIAL DISCRIMINATOR
BIASED AMPLIFIER AND GATE GENERATORS
AMPLIFIER AND PULSE SHAPERS
PRECISION PULSER FED INTO 1ST GRID OF PREAMP
XTAL, PHOTOTUBE, AND PREAMP

FIGURE 7

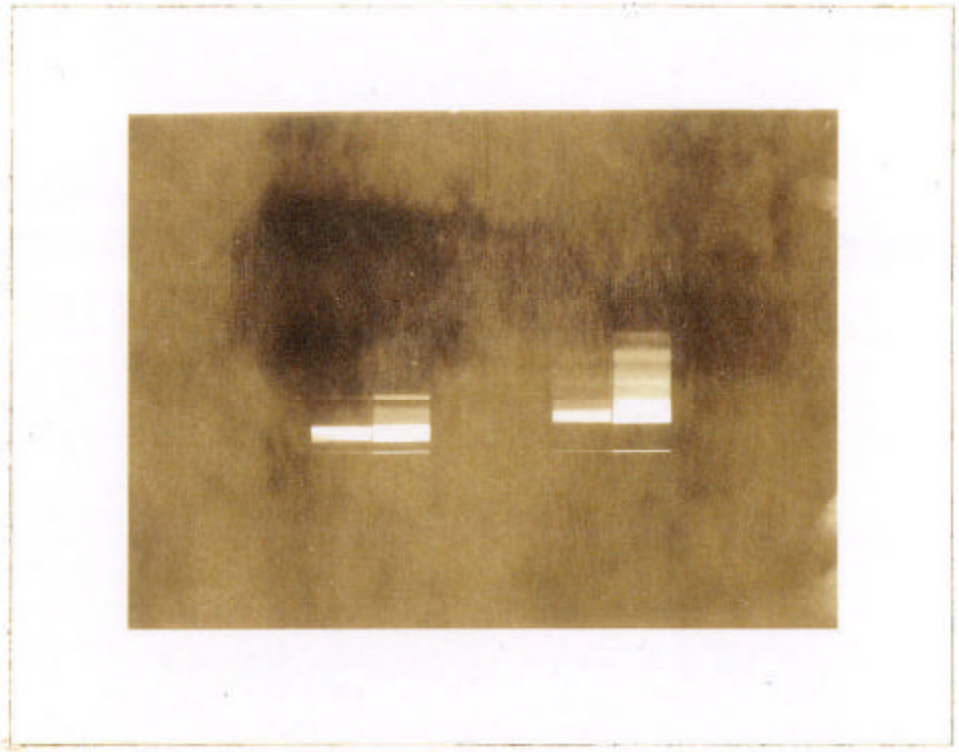

FIGURE 8

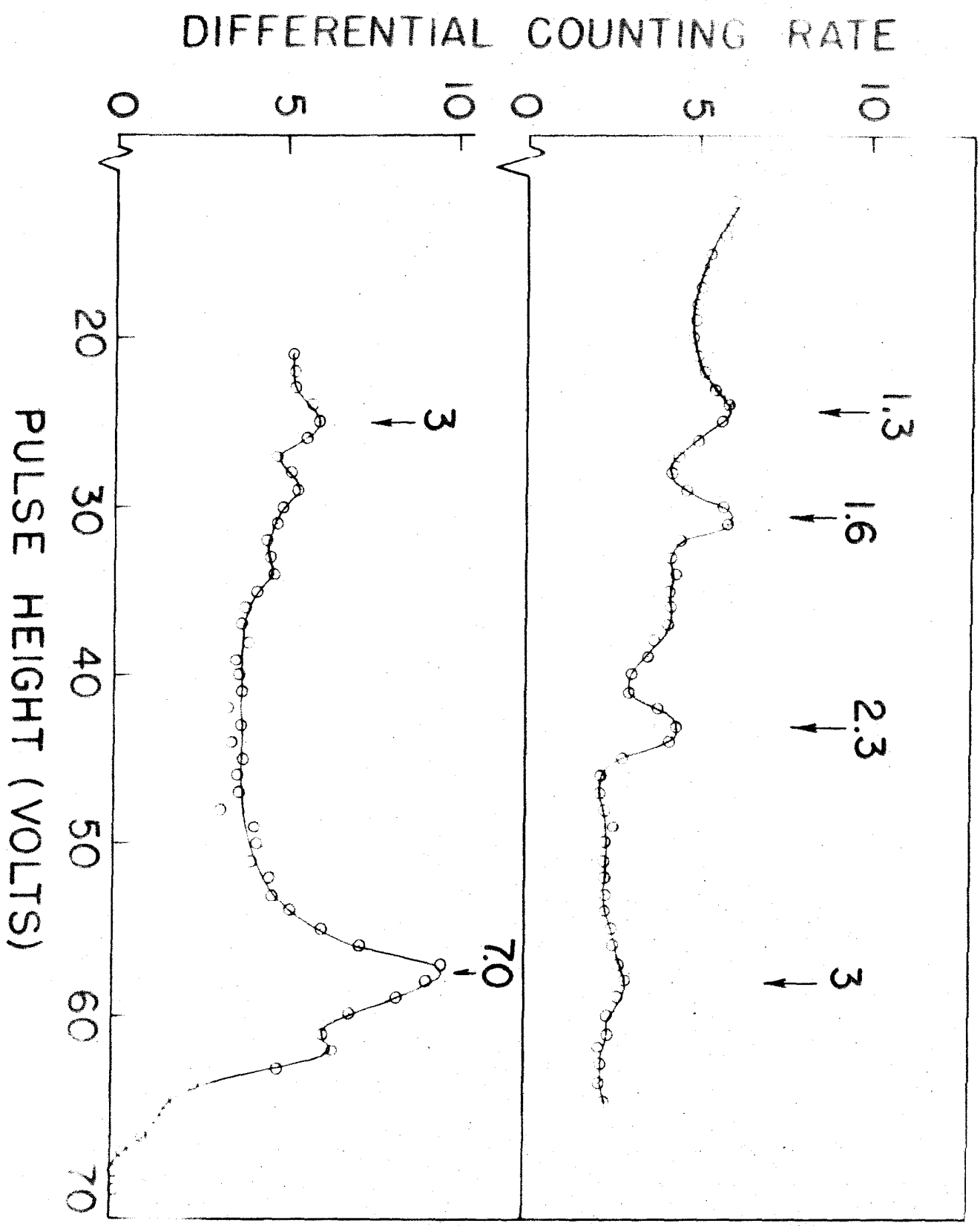
DIFFERENTIAL COUNTING RATE
0
5
10
0
5
10
PULSE HEIGHT (VOLTS)
20
30
40
50
60
70
3
7.0
1.3
1.6
2.3
3

Figure 9

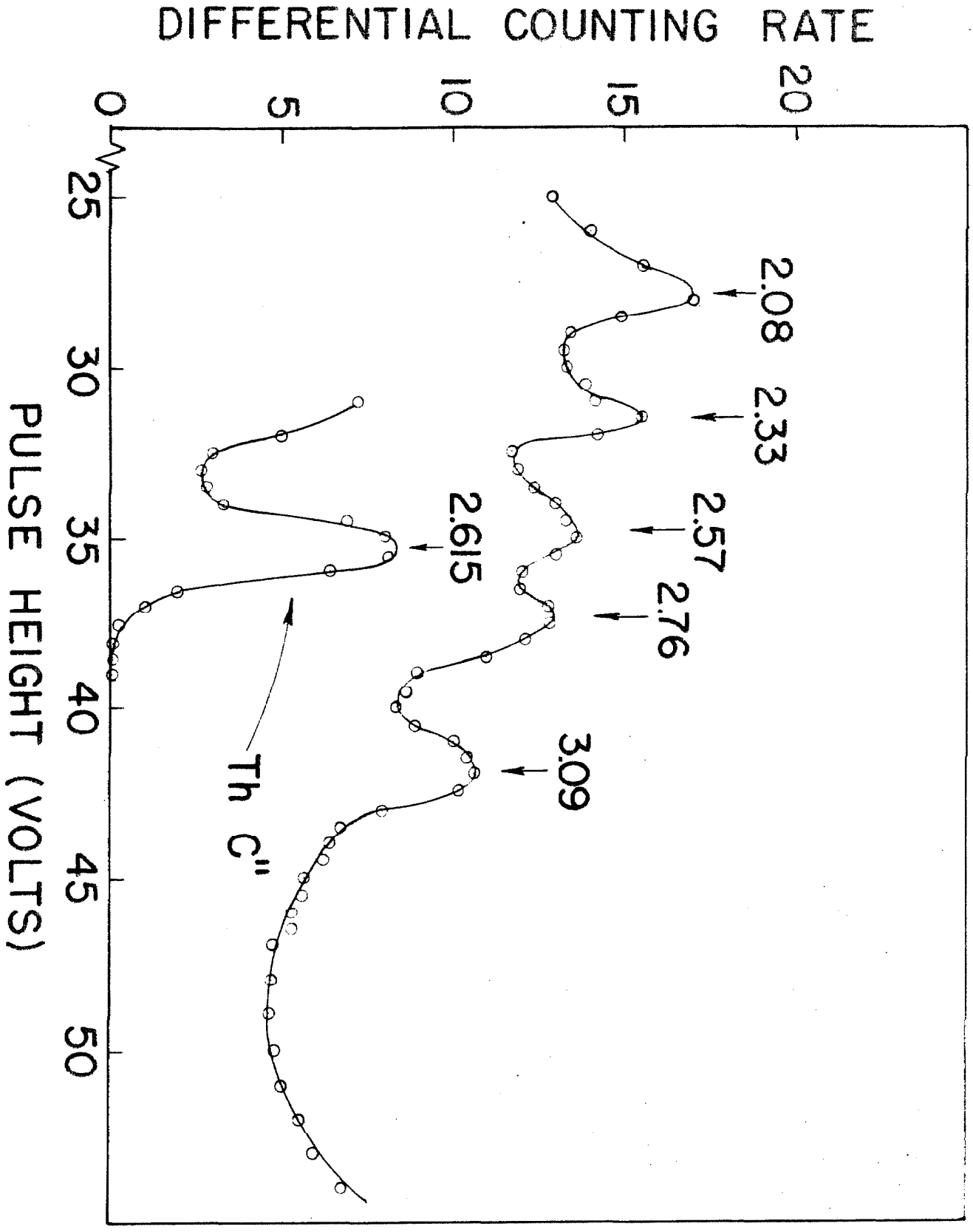
DIFFERENTIAL COUNTING RATE
0
5
10
15
20
25
30
35
40
45
50
PULSE HEIGHT (VOLTS)
2.08
2.33
2.57
2.76
3.09
2.615
Th C''

Figure 10

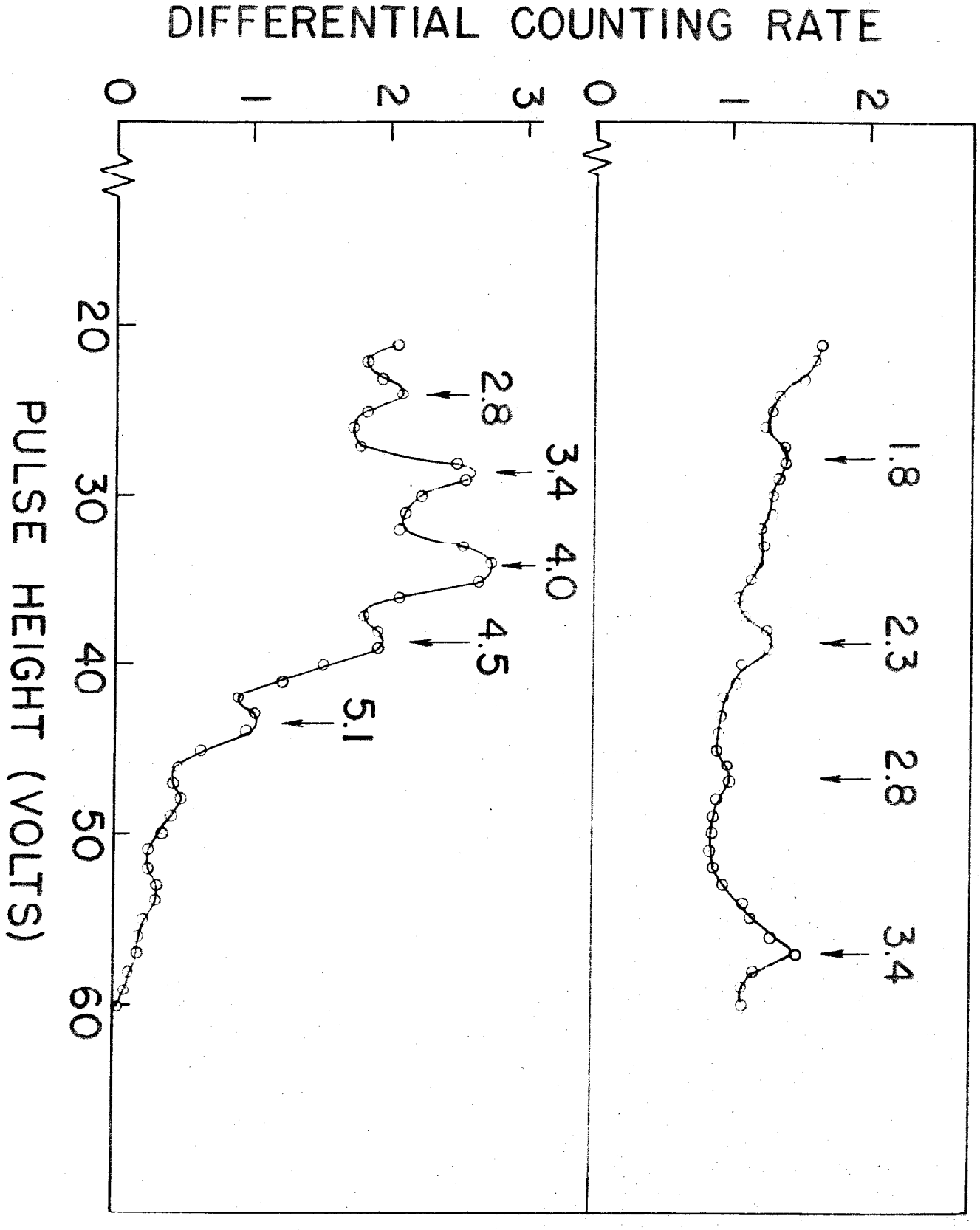
DIFFERENTIAL COUNTING RATE
0
1
2
3
0
1
2
PULSE HEIGHT (VOLTS)
20
30
40
50
60
2.8
3.4
4.0
4.5
5.1
1.8
2.3
2.8
3.4

Figure 11

Ep=2.10
9.49
Ep=1.76
9.17
10±2
90
Ep=1.55
8.98
Ep=1.46
8.90
Ep=1.25
8.70
10
90
14±5
27±5
59
8.62
Ep=1.16
11±2
89
8.06
Ep=0.55
6.44
35±10
65
5.81
74
26±4
5.08
34±6
66
3.95
2.31

FIGURE 12

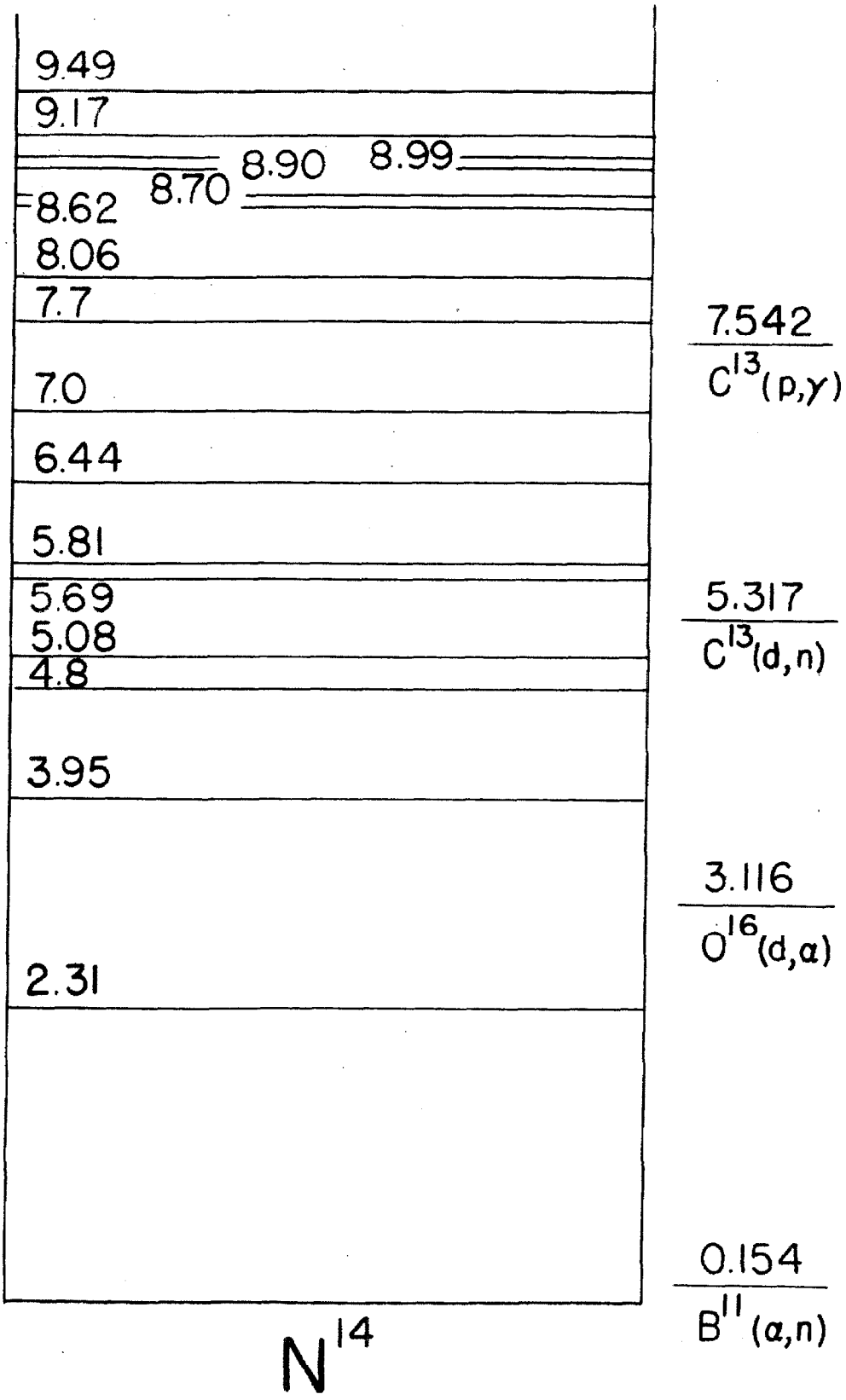
9.49
9.17
8.99
8.90
8.70
8.62
8.06
7.7
7.542
C13(p,γ)
7.0
6.44
5.81
5.69
5.08
5.317
C13(d,n)
4.8
3.95
3.116
O16(d,α)
2.31
0.154
B11(α,n)
N14

FIGURE 13

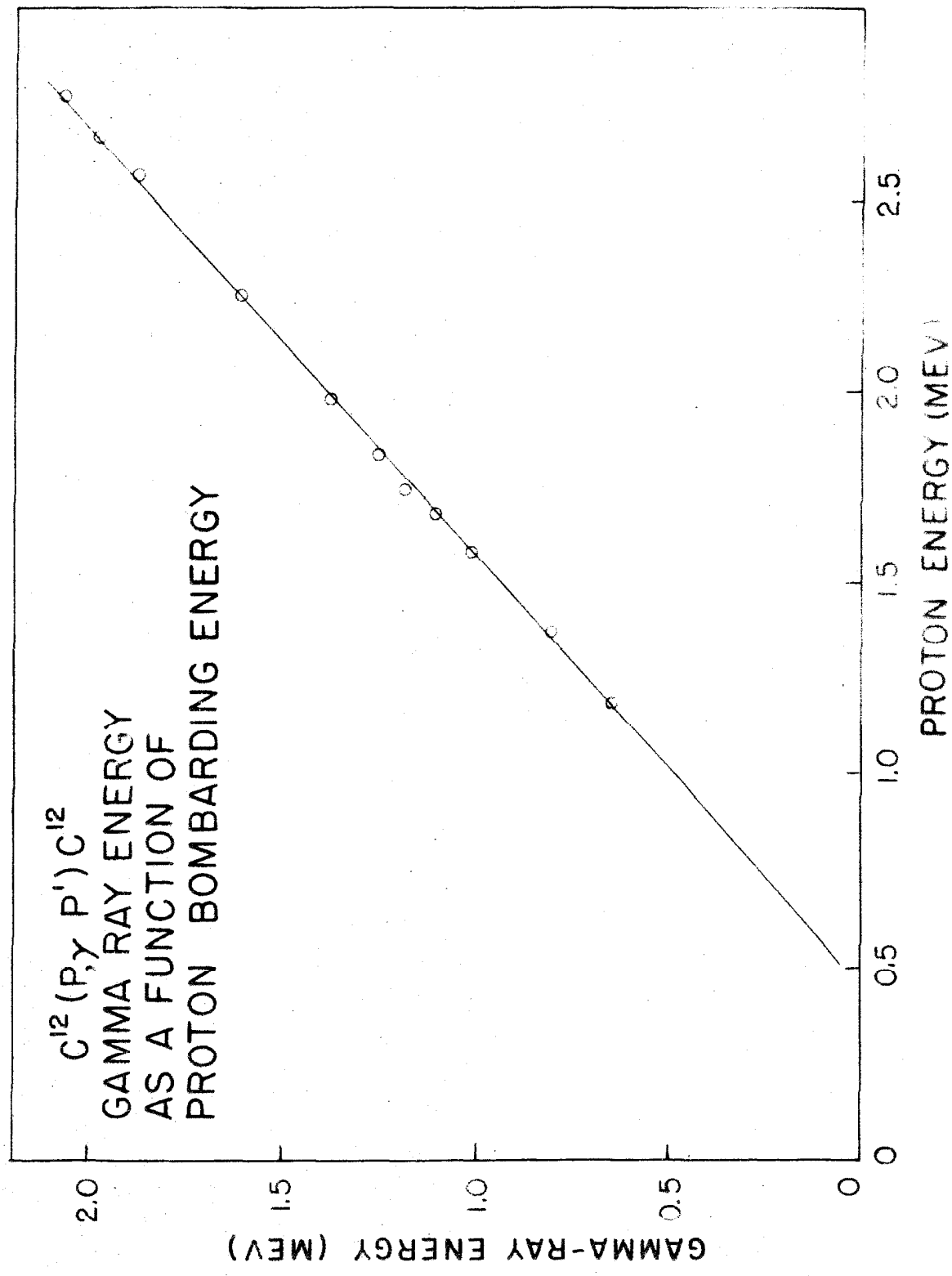
$C^{12}(P,\gamma\ P')C^{12}$
GAMMA RAY ENERGY
AS A FUNCTION OF
PROTON BOMBARDING ENERGY
GAMMA-RAY ENERGY (MEV)
PROTON ENERGY (MEV)
0
0.5
1.0
1.5
2.0
2.5

FIGURE 14

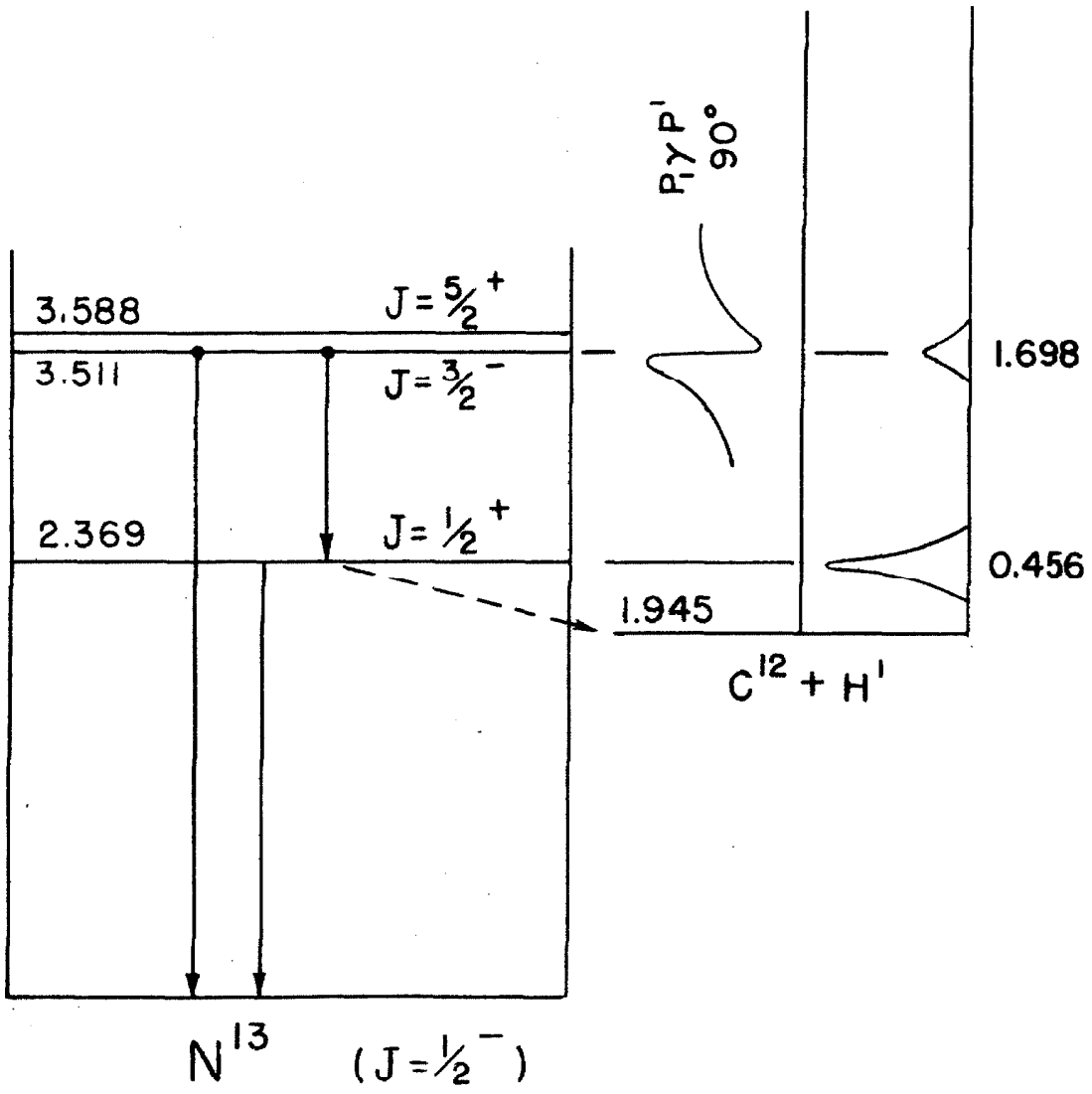

FIGURE 15

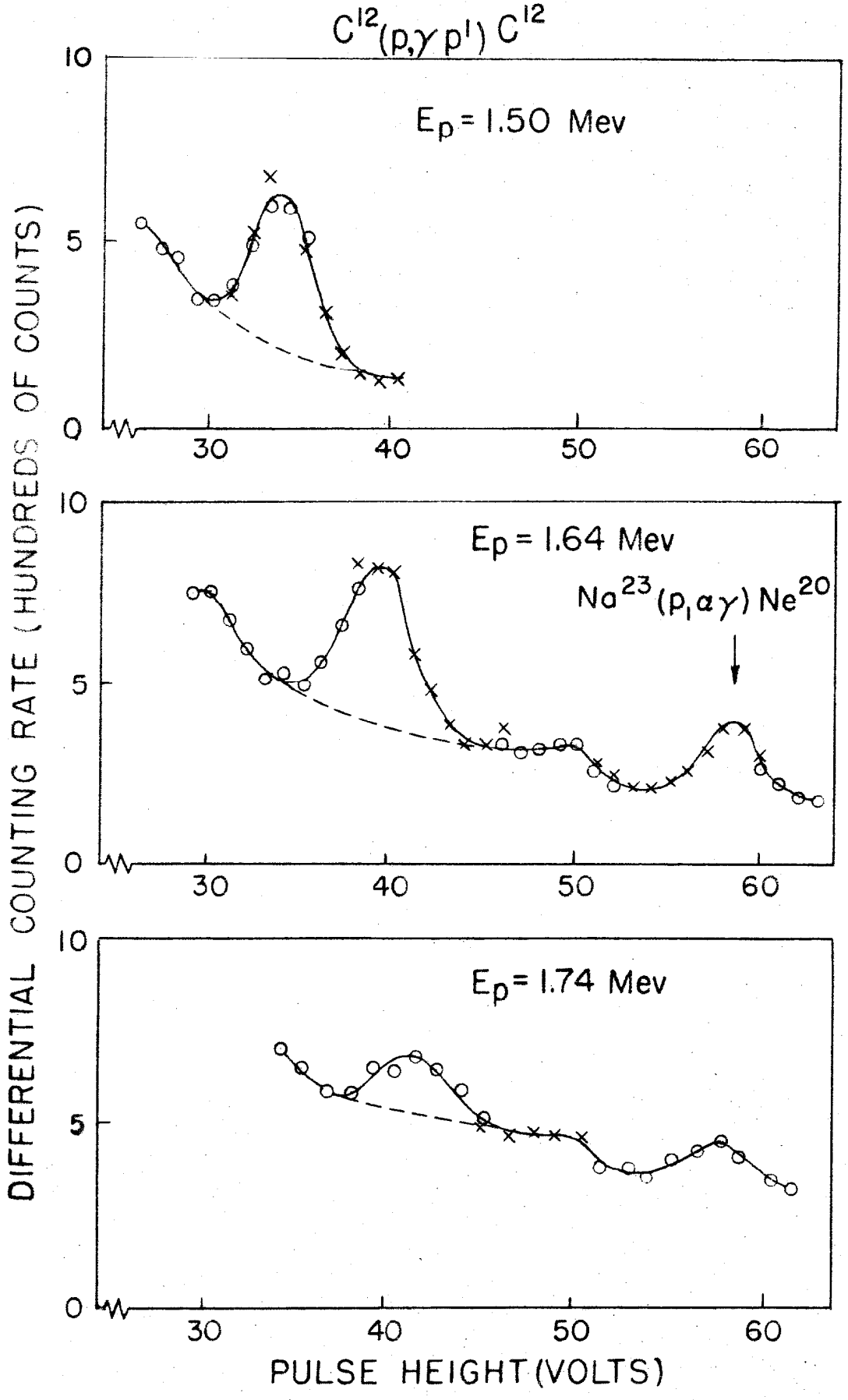
$C^{12}(p,\gamma p')\,C^{12}$
E_p = 1.50 Mev
E_p = 1.64 Mev
$Na^{23}(p,\alpha\gamma)\,Ne^{20}$
E_p = 1.74 Mev
DIFFERENTIAL COUNTING RATE (HUNDREDS OF COUNTS)
PULSE HEIGHT (VOLTS)
0
5
10
30
40
50
60

Figure 16

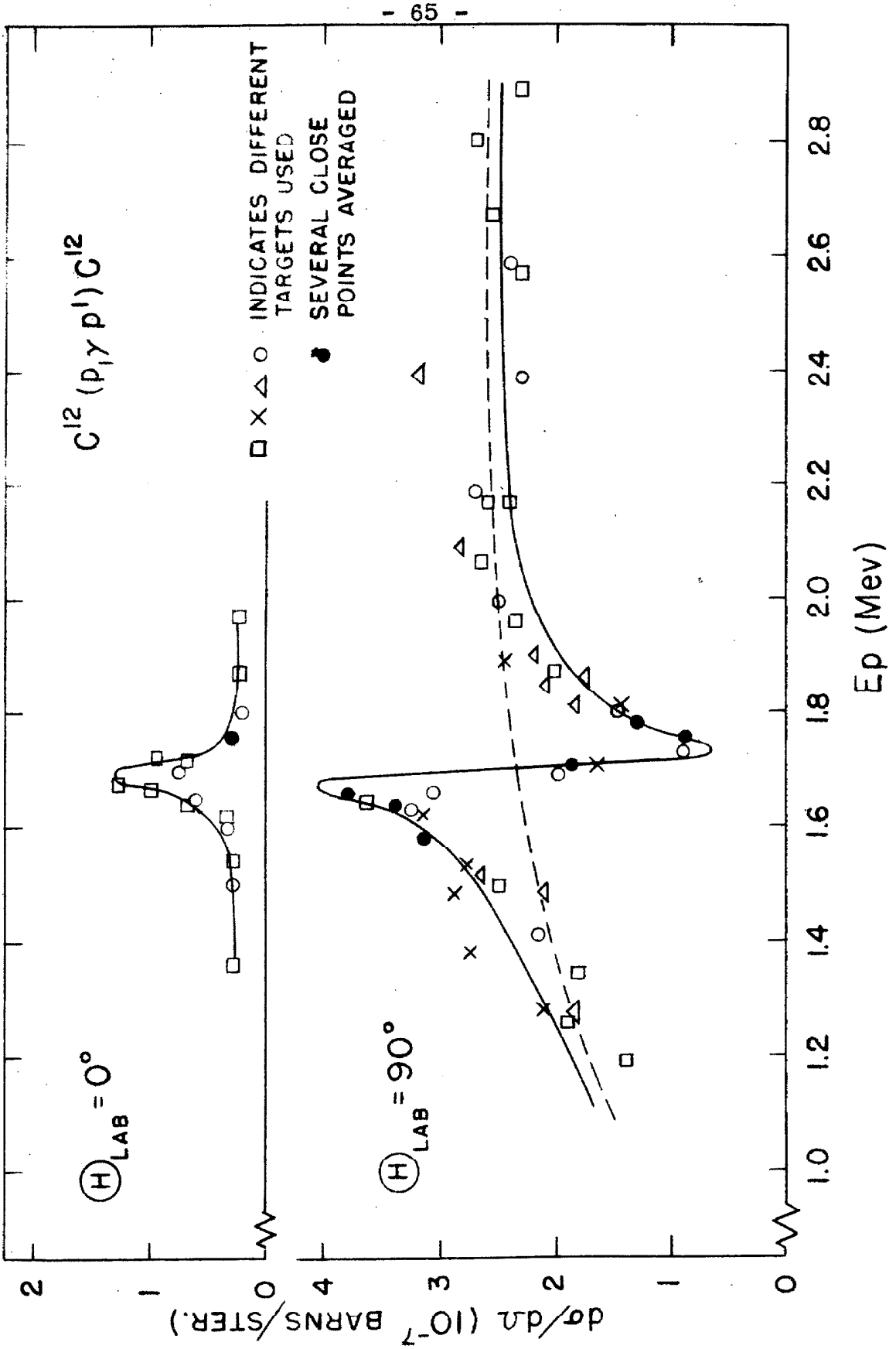
$C^{12}(p,\gamma p')C^{12}$
□ × △ ○ INDICATES DIFFERENT TARGETS USED
● SEVERAL CLOSE POINTS AVERAGED
$\theta_{LAB}=0°$
$\theta_{LAB}=90°$
$d\sigma/d\Omega$ (10^{-7} BARNS/STER.)
Ep (Mev)
0
1
2
3
4
1.0
1.2
1.4
1.6
1.8
2.0
2.2
2.4
2.6
2.8

FIGURE 17